Development and Investigation of Semi-active Haptic Interfaces Using Digital Resistance Map Concept

by

Ehsan Asadi

B.Sc., Shiraz University, 2010

Thesis Submitted In Partial Fulfillment of the
Requirements for the Degree of
Master of Applied Science

in the
School of Engineering Science
Faculty of Applied Sciences

SIMON FRASER UNIVERSITY

Fall 2012

Approval

Name: **Ehsan Asadi**

Degree: **Master of Applied Science**

Title of Thesis: ***Development and Investigation of Semi-Active Haptic Interfaces Using Digital Resistance Map Concept***

Examining Committee: **Chair:** Dr. Gary Wang
Professor

Dr. Siamak Arzanpour
Senior Supervisor
Assistant Professor _____

Dr. Mehrdad Moallem
Supervisor
Professor _____

Dr. Krishna Vijayaraghavan
Internal Examiner
Assistant Professor _____

Date Defended/Approved: December 07, 2012

Partial Copyright Licence

Abstract

The growing demand for haptic technologies in recent years has motivated novel approaches in developing haptic interfaces and control algorithms. Based on the force reflecting nature and energy flow directions, those interfaces are categorized in active and semi-active groups. Semi-active interfaces, in general, have the advantage of addressing safety concerns which adversely affects their active counterparts. This thesis presents the development of semi-active haptic interfaces using Magnetorheological (MR)-dampers. The ability of MR-Dampers in producing controllable resistance forces is the key reason for their utilization in interfaces. Our semi-active haptic interfaces are consisted of linear and rotary MR-Dampers. Each of the MR-Dampers is modeled using Bouc-Wen model. The parameters of the mathematical equation of the MR-Damper are identified experimentally. The concept of Digital Resistance Map (DRM) is developed as main strategy for activating MR-Dampers for semi-active interfaces. A preliminary study is carried out to verify the potentials of MR-Dampers and DRM for implementing in semi-active haptic system. Next, the DRM concept is expanded and introduced as a haptic rendering algorithm. The DRM is a high-fidelity haptic rendering algorithm and proved to be effective to create comprehensive force feedback for operators. MATLAB/Simulink is used for implementing several DRM scenarios for generating haptic enabled virtual environments. Several experiments are conducted to demonstrate the effectiveness of the interface and rendering algorithm. A human subject experiment is also included as a further investigation of the proposed system. The interface is integrated with virtual reality to provide the human operators with haptic and visual feedbacks. The obtained results confirm that the proposed system is able to generate understandable haptic and visual feedbacks to help the operators to explore virtual environments. Also, it is found that, to obtain the best human performances, haptic and visual feedbacks need to be combined.

Keywords: Haptics; Display Algorithm; Digital Resistance map; Semi-active; MR-Damper; MR-Damper Modeling

Dedication

To my beloved parents

Acknowledgements

First and above all, I praise Allah, God Almighty, for providing me this opportunity and granting me the capability to proceed successfully.

I am extremely grateful to my parents ,Abdolazim Asadi and Farkhondeh Mohammadi, for their love, prayers, caring and sacrifices and continuing support for educating and preparing me for my future. My appreciation likewise extends to my brother Ali and my sister Nahid for unflagging love and support throughout my life.

This dissertation would not have been possible without the guidance and the help of several individuals who in one way or another contributed and extended their valuable assistance in the preparation and completion of this study. First and foremost, my utmost gratitude goes to my senior supervisor Dr. Siamak Arzanpour, for his inspirations and guidance throughout my research. I am also indebted to my supervisor, Dr. Mehrdad Moallem, for his support. I would also like to thank Dr. Vijayaraghavan for kindly reviewing the thesis. I would like to extend my gratefulness to Dr. Wang for his time and energy as my session defence chair.

All my friends in Vancouver made it a convivial place to live. They were and are like a family to me. In particular, I would like to thank Hossein, Hamidreza, Moein, Mehdi, Mohammadreza, Hanieh, Tayebeh and Vahid for their friendship and help in the past few years. Thank you for inspiring me in research and life during the hard days in Vancouver.

Table of Contents

List of Tables

List of Figures

1. Introduction

Haptic refers to technologies that provide sense of touch as a new source of information for interfaces to enhance human interactions with environment. The effectiveness of these technologies is usually assessed by measuring how much more sense of presence will be felt by the users, if they are added to interfaces. As defined by Witmerer al, [1], sense of presence is the users' feeling of being in other environments than what they are located at. By providing this feeling, interfaces enable the users to explore virtual environments in computer simulations and to operate in remote environments in telerobotic operations. Traditionally, interfaces rely only on visual and auditory information to generate sense of presence for the users. With the incorporation of new electronic technologies, significant improvements in terms of sense of presence have been brought into these interfaces. Much better sense of presence in the virtual or remote environments, however, is feasible if these interfaces can be synchronized with Haptics [2]. Haptic equipped interfaces are aimed to provide the users with tactile and kinesthetic information as a complementary feedback channel. By capturing and regenerating mechanical signals, such as force [3], motion [4] and vibration [5], users not only see and hear but also feel what is happening in the environments [6].

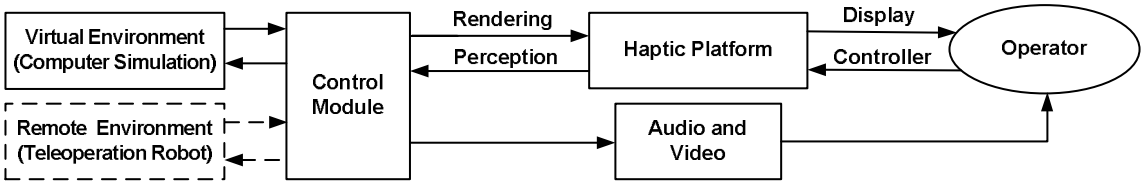

Figure 1: A schematic view of haptic systems.

Figure 1 is a schematic view of a typical haptic system which enables an operator to interact with an environment. To relocate inside the environment, the operator applies force and motion to the haptic platform. The haptic platform is a mechanical device that is equipped with suitable sensors to acquire the operator's

controlling inputs. The controller interprets these signals and uses them to explore the environment by manipulating an end-effector. The interacting environment can be remote or virtual. Remote environments are real but usually inaccessible or hazardous; therefore, a telerobot is steered inside the remote environment to do tasks. Telerobots end-effector(s) is the representative of the operator hand and thus is equipped with sensors to measure the gripping force. Virtual environments, on the other hand, are computer simulated 3-dimentional environments that a virtual end-effector is utilized to manipulate inside a virtual environment to interact with objects. Computer simulator uses end-effector position and geometrical properties of virtual environment to numerically detect collisions and penetrations. In both cases, once the interaction information is obtained from the environment, they need to be converted into haptic scenes (virtual physical scenes). To do this, the controller is programmed with a display rendering algorithm (DRA). DRA receives the interaction information and renders them into haptic scene. Computed haptic scenes are then shown on the haptic platform by means of generating proper mechanical signals for the human user.

Haptic technologies are often multidisciplinary and their developments require collaborations of experts from various areas. Haptic interfaces have a broad range of applications. One of the most commercially demanded areas of their application is computer gaming [7]. Joysticks and wearable haptic controllers are now designed to bring realistic feeling of virtual environments and enhance computer games market. Moreover, Haptics has increased the hope for the future development of computer games for visually impaired people [8, 9]. CAD/CAM and NC machines are also benefiting from haptics in their tool path planning, tool orientation determination and tool collision avoidance [10]. Virtual prototyping is another example of CAD/CAM that Haptics can assists. Virtual prototyping is a method that involves the integration of virtual reality with other technologies to produce digital prototypes. The realism of such systems can be enhanced by means of haptic interfaces [11]. Telerobotic surgery is another emerging area of haptic interfaces where high precision manipulators are employed to conduct real-time operations [12-15]. In those applications, haptic interfaces are integrated with the robotic systems to compensate for surgeons' lack of tactile sense [16, 17]. Haptic interfaces are also customized for physical therapy and rehabilitation. Specialized robots are designed and programmed to retain muscle functionality by applying controlled

forces to patients' organs and correcting the exercises recommended by therapists [18-20].

The efficiency of haptic systems highly depends on the ability of platforms to generate mechanical signals. To generate the signals, different mechanical actuators can be employed. Depending on feedback type and energy flow directions, haptic display platforms are categorized as active and semi-active. In active haptic interfaces, the energy flow between an operator and an interface is bi-directional. In those interfaces, active actuators such as electric motors and pneumatic/hydraulic cylinders are employed for producing a virtual physical environment by applying force to imply the effect of barriers, obstacles and walls [21-23]. Stability, transparency (feeling of direct interacting with the virtual/remote environment [24]), and operation safety are some of the factors that limit the application of active haptic interfaces [25].There is a tradeoff between high transparency and sufficient stability margins. The feedback of large signals, generated from environment interactions, will introduce instability in the system; however, weakening these signals will result in a non-transparent system. Although, stability and transparency issues has been tried to be addressed by introducing a number of approaches, such as increasing sampling rate [26], virtual coupling [27] and discrete-time signal processing techniques [28] , the issue of safety in active interfaces is still a major concern. This is mainly because the actuators are able to apply forces and hence the risk of potential damages to injured or disabled human subjects cannot be entirely eliminated. Safety of active haptic interfaces can be enhanced by using high-end actuators and developing more reliable controllers; however, incorporating all these features increase the cost of the system [19]. In semi-active haptic interfaces the flow of energy is from the operator to the haptic interface and hence the device operation is safe [27]. In those systems, the motion resistive actuators are utilized to create haptic scenes. Active and semi-active haptic interfaces have particular advantages that make each of them viable for specific applications. In summary, semi-active systems are low cost, safe, and stable, and active systems have bi-directional energy flow.

One of the other key factors that directly affects the effectiveness of both of active and semi-active interfaces is the fidelity of haptic rendering algorithm. It is important that the pattern of generating the haptic scenes follows a practical algorithm, such that the scene is understandable for operators, and effectively guide them to

explore the virtual environment. This issue is highlighted more for semi-active interfaces. In those interfaces, no active force is available to correct the motion. Users rely only on resistive (not active) forces for guidance and therefore, they should correct the motion if required. Consider the case of intruding into a virtual wall as an example. In active interfaces, the user hand is pushed back against the wall. This means that the actuators automatically return the user hand to the wall surface. In a semi-active interface, however, no active force is available to correct the motion and during the penetration, the hand motion is only resisted. The pattern of generating resistance in semi-active interfaces thus needs to follows a practical algorithm, such that the feedback is understandable for users, and effectively guides them back to the surface. Otherwise, the user gets confused and trapped in the wall. In this research, the main objectives are 1) designing and investigating the performance of a semi-active haptic interface, and 2) developing an understandable haptic rendering algorithm that is compatible with semi-active interfaces.

Our interest in developing a new haptic rendering algorithm for semi-active systems is primarily motivated by the need in rehabilitation for having a versatile, cost effective but safe and user-friendly haptic interface that can assist patients in regaining their functionality. Based on this need, in chapter two, a preliminarily study is carried out to validate the feasibility of using semi-active haptic interfaces for rehabilitations robots. The haptic device that is designed in this preliminarily study addresses the issue by employing MR-Dampers and a user-friendly programming methodology. The concept of Digital Resistance Map (DRM) is introduced as main strategy for controlling MR-Dampers and restricting the motion to the regions determined by the therapist. To simulate the performance of the system, an accurate model of MR-Damper is obtained and validated experimentally. To test the performance of the proposed MR-based haptic device, the resistance maps are first generated. MR-Dampers are activated according to the positions of the end-effector in the resistance map. The system is also simulated in MATLAB/SimMechanics. The experimental and simulation results are in good agreement. The promising results of this study make the proposed haptic interface and DRM concept potential candidates for rehabilitation applications.

The simplicity and effectiveness of the DRM concept in controlling MR-Dampers and generating haptic scenes also motivated us to further investigate its potentials as a

new display rendering algorithm (DRA) for semi-active haptic interfaces. Chapter 3 further expands on the development of the DRM as a simple yet understandable DRA. In chapter 2, The DRM uses only end-effector position parameter to calculate desired resistance forces. In chapter 3; however, a force sensor is also implemented in the haptic platform to measure operators input force. Including force information in the computations enables the DRM to detect the direction of the motion easier. It also helps to provide higher resistance force resolution through a feedback control. Experimental verifications for the effectiveness of the enhanced DRM in computing and generating haptic scenes using semi-active haptic interfaces are presented. An experimental polar semi-active haptic interface is designed and fabricated using a rotary and a linear MR-Dampers. The mathematical model of the semi-active system is first obtained and then used in the controller software developed in MATLAB/Simulink environment. Extensive experimental results presented in this chapter demonstrate the effectiveness of proposed semi-active haptic interface and the DRM methodology as a DRA.

Chapter 4 is dedicated to testing the effectiveness of the system on human subjects. Ten participants from university students are asked to execute two series of tasks under different combinations of haptic and visual feedbacks. To evaluate the merits of our system, the error of those tasks under different feedback conditions is analyzed by box plots and ANOVA methods. It is proved that the proposed haptic system is able to enhance the accuracy of performed tasks.

2. Developing an MR-Damper Based haptic Platform for Rehabilitation Exercises

In this Chapter, the need for developing new rehabilitation robots to address safety and versatility concerns of traditional rehabilitation systems is explained first. A planar MR-Damper based haptic interface is then proposed to cover the concerns. Furthermore, concept of Digital Resistive-Map (DRM) is introduced as potential strategy for controlling MR-Dampers.

2.1. Application of Haptics in Rehabilitation

Muscle functionality, which defines human mobility, depends on several factors including age. It can be altered due to potential physical damage imposed by injuries or stroke. The lack of muscle functionality will impose significant cost to patients and the healthcare system [29]. Usually, rehabilitation devices are designed to assist individuals to retain their muscle functionality [30]. They help patients to retain muscle functionality by restricting the muscle motion to a region or trajectory predetermined by therapist in repetitive exercises. Recently, the presence of haptic based robots in rehabilitation has shown a significant growth [31,32].The main advantages of haptic based robotic therapy are repeatability and online measurement [33]. Repeating prescribed exercises is shown to help retaining muscle functionality, and online measurement enables the physiotherapists to more carefully monitor the healing process and adjust the exercises to get the best results. In robotic rehabilitation, therapists' recommended motion trajectories can be programmed in a virtual environment and implemented with actuators in reality by applying force to constraint motion.

Design of reliable robotic systems is one of main concerns in field of rehabilitation. Some rehabilitation robotic devices are meant to aid strength development of specific motor movements, while others seek to aid these movements directly. These

devices include exoskeletons, enhanced treadmills such as Lokomat, and robotic arms, and MIT-MANUS. Veras *et al*. [34] have also developed a rehabilitation system to give assistive force feedback through a haptic controller to the user for performing repetitive task. Their system also can be incorporated in teleoperation manipulations. Kikuchi *et al*. [35] designed a 6-Degree of Freedom (DOF) upper rehabilitation system integrated by virtual reality technology, and utilized it to train stroke survivors. They also made a model of movement of stroke survivors and healthy people by measurement and based on the model, they developed a software for training purposes.

In rehabilitation robotic safety is indispensable, e.g. excessive forces are needed to be eliminated, and this issue should be considered in mechanism design as well as controller development. Besides, the patients need to feel safe to use the device. [36, 37]. For example, false fear of using haptic rehabilitation robots, caused by unexpected movements of the device, is a common experience for many patients. Reliability of active haptic interfaces can be increased using high-end actuators and developing controllers that address higher safety requirements (e.g. force feedback); however, implementing all these safety features adds to the cost of the device and will make it not affordable for many care facilities. Although the risk of damage can be minimized, there is no guarantee for its elimination. Moreover, the lack of expertise of therapist with programming the device limits its application to some pre-programmed options. Also, the patients are required to come to the care facility for the exercises. Having versatile, inexpensive, and user-friendly assistive devices that are safe to be operated by the patients at their homes without supervision and are convenient to be reprogrammed and monitored remotely by therapists will be of high demand. Such devices should have the maximum safety which indirectly implies that no actuation force is allowed [30].

Among all actuators, semi-active dampers are potentially the best candidates. They are only able to generate resistive (not actuation) forces and hence are safe for the users.[38]. In additions, they are cheaper than linear motors, and will last longer [39, 40]. Magnetorheological (MR) and Electrorheological (ER) dampers are the two major types of actuator that can be potentially used for semi-active interfaces. In general, MR-Dampers have higher yield stress, larger operable temperature and better tolerance for the fluid impurities [41, 42].

The application of MR-fluid in semi-active haptic interfaces is first investigated in the early 2000s. Scilingo *et al*. [43, 44] showed that such devices are able to imitate the compressional compliance of biological tissues for surgical training in minimally invasive surgical applications. Since then, a number of semi-active based haptic interfaces have been proposed for various applications including human-vehicle interface [45], telerobotic surgery [46], and rehabilitation [47]. In most cases, MR-Dampers are customized for specific requirements of operations. For example, the MR-Damper based rehabilitation robot proposed by Nikitczuk *et al*. [47] is designed specifically for gait retraining in stroke patients and cannot be employed for other cases. This shortcoming can be addressed by designing higher degrees of freedom MR-damper based semi-active systems. Ahmadkhanlou *et al*. [24, 46] have developed a 5-DOF MR-Damper based serial robotic arm (the master) that is employed to control a remote 5-DOF motorized robot (the slave). Their system is capable of performing different surgical operations.

In this chapter, a novel MR-Damper based planar haptic interface is proposed for rehabilitation application. Two linear MR-Dampers are used in this design. The general idea of this device operation is generating regions in the device workspace (called Resistance Map) with different resistances to motion through activating the dampers. A mathematical model of the MR-Damper is derived and validated experimentally. This model is implemented in MATLAB/SimMechanics for MR-damper haptic interface simulation. An experimental setup of the haptic interface is also developed and its performance is compared with simulation models.

2.2. Digital Resistance Map Concept: an Answer for Haptic Based Rehabilitation Exercises

The main objective of physical therapy is to retrain the functionality of weak muscles by constraining motions in repetitive exercises [48, 49]. Physiotherapists target specific groups of muscles and plan for the best exercise to train them. These exercises will be selected carefully to exclude neighbouring muscles. Depending on disabilities and damages, muscle movement is only allowed along recommended trajectories. To reduce the risk of further damages, any excessive force on the muscle during the exercises

must be avoided. These concerns are traditionally addressed by developing devices that guide body organs' movement through certain trajectories. For instance, in arm therapy, hand will be allowed to move in certain directions in a workspace to maximize the likelihood of using specific muscles. This workspace can be generated as regions with distinct resistances against motion. In this research, such workspace is called resistance map and the borders for each of the regions are named resistance boundaries. Figure 2 demonstrates this concept by showing a resistance map and resistance boundaries.

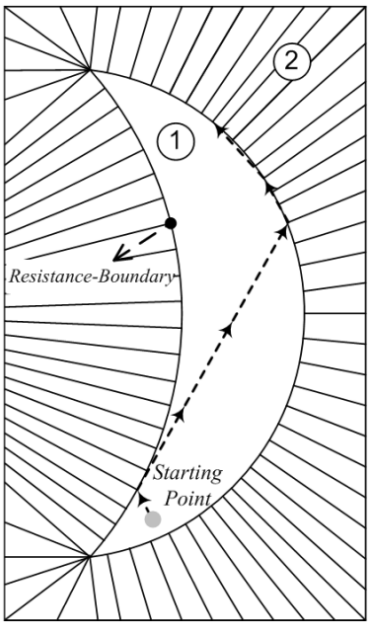

Figure 2: A schematic view of resistance map and resistance boundaries.

In this map, the middle region has no resistance so motion is not restricted inside it (authorized region). This region is surrounded by a media that has high resistance to motion (prohibited region). To better visualize the idea of Resistance Map, an example can be given by assuming a ball is thrown inside region 1. The ball will move in a straight line until it hits the resistance boundary where its motion is blocked inside region 2. Therefore, the ball selectively turns back inside region 1 and it does the same each time it hits the resistance boundary. Resistance Maps can be generated either by physical constraints or using actuators. They also can be customized according to different kinds of disabilities. For example, Colombo *et al*. [29] presented a wrist rehabilitation device that constraint body organ motion to an arc of a circle. In another example, Rahman *et*

al. [50] developed a wearable robot for rehabilitation of elbow and shoulder joint movements in which motion is restricted to be in a vertical plane and any motion outside this plane is prohibited. In all of these applications, motion restriction is achieved by permanent physical constraints, therefore significant modifications or perhaps new constraint designs are required to adopt the devices for other types of disabilities. Although physical constraints might be inexpensive solution, actuators bring lots of versatility to the equipment, so the maps can be reconfigured by programming. MR-Dampers are semi-active actuators that can be used for this application. These devices can produced large resistive (no actuation) forces proportional to applied current. To cover planar resistance-maps, two MR-Dampers will be sufficient. The configuration of a planar system is shown in Figure 3.

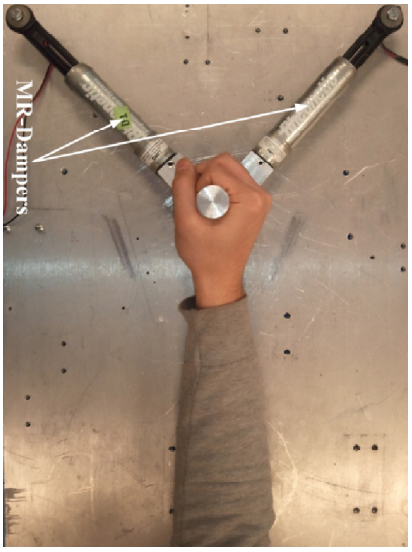

Figure 3: MR-Damper haptic interface for rehabilitation application.

The procedure for producing a physical Resistance Map begins first by its digitization into a virtual environment and then synchronizing that with the workspace of MR-Dampers platform. A virtual end-effector in the virtual environment represents the position of hand inside the platform workspace. To synchronize the damper platform and the digital resistance map, two position sensors are used to measure the location of hand. According to the motion of hand, the virtual end-effector relocates in the digital map. A controller is developed to activate MR-Dampers to produce the resistance against motion based on the resistance map requirement at end-effector location.

2.3. Mathematical Modeling of MR-Damper

The accuracy and effectiveness of the Resistance Map depends on the performance of the controller. To develop such control, mathematical models of the MR-Dampers are needed. MR-Dampers are semi-active actuators which their damping characteristic can be adjusted by controlling the supply electric current of the coils. The capability of producing controllable damping force in MR-Damper is an appealing characteristic for many applications including civil engineering structures [51], automotive suspensions [52] and haptic rehabilitations [47]. MR-Dampers are highly non linear which makes their modeling and control challenging. Their force is a function of several variables including their design, excitation characteristics (i.e. velocity and acceleration), and applied current [53, 54]. Modeling MR-dampers has been investigated by many researchers and several models have been proposed for capturing their dynamic behaviour [42], [55-57]. In this study, Bouc-Wen model is selected because it can effectively capture the essential dynamical behaviour of MR-Dampers. The model is also not complex and numerically tractable (can be solved using numerical methods for real-time control systems) [58].

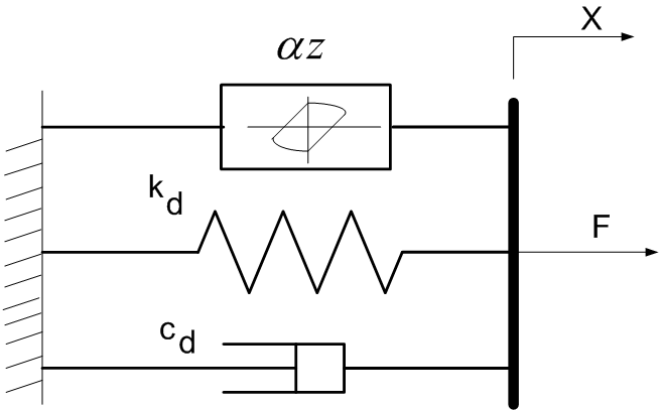

Figure 4: Bouc-Wen model (Spencer, 1997).

Figure 4 shows a diagram of Bouc-Wen modeling. In this model, the resistance generated by the device is given by the following equations,

$$F(x,\dot{x}) = K_d x + C_d \dot{x} + \alpha z \quad (1)$$

$$\dot{z} = A\dot{x} - \gamma|\dot{x}z^{n-1}|z - \beta\dot{x}|z^{n}| \qquad (2)$$

Where x is the displacement of MR-Damper, z is the damping force evolutionary variable,K_d, A, γ, β and n are constant parameters, and C_d and α are usually functions of applied current. An algorithm is developed to find the parameters for this particular damper from experimental measurements. In order to identify the model parameters, a cost function J is defined as [38]:

$$J = \sum_{i=1}^{N} (F_{ex}(t_i) - F_{md}(t_i))^2 \qquad (3)$$

Where F_{ex} refers to experimental forces and F_{md} refers to modeling forces obtained from numerical solution of the model using the Runge-Kutta integration method.

The utilized linear MR-Damper is a RD-1097-01 MR-Damper made by Lord Co and its specification is summarized in Table 1.

Table 1: Linear MR-Dampers specifications.

compressed length (mm)	extended length (mm)	maximum continuous working current (A)	maximum intermittent input current (A)
195	253	0.5	1

An experimental setup as illustrated in Figure 5 is designed. In this setup, an electromagnetic shaker (LDS 722) is used to produce excitation. MR-Damper is attached to a fixed plate on top and to the shaker from its other end. An LVDT and a load cell are used to measure the relative displacement and the damping force of the damper.

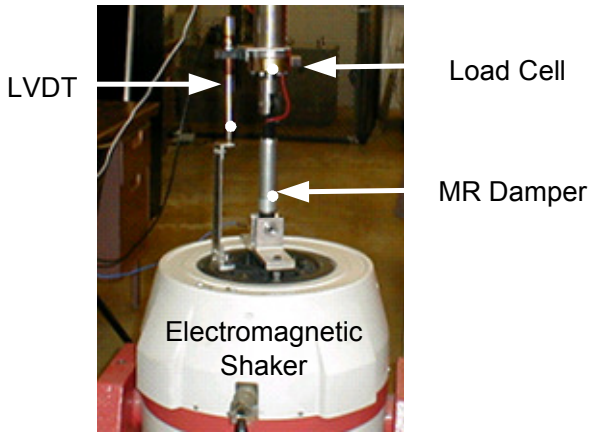

Figure 5: Experimental setup for testing MR-Damper.

The damper is tested under several conditions using sinusoidal input. Excitation frequencies are selected between 6-8 Hz and the amplitudes 3-5 mm, respectively. The applied electric current values are set at 0.0, 0.10, 0.20, 0.30, and 0.35 A. The Bouc-Wen model parameters were determined by minimizing the cost function with the MATLAB genetic algorithm toolbox. The dampers parameters are identified as,

$$[K_d, A, \gamma, n, \beta] = [0, 36.2095, 10.6140, 1, -7.0773\ ] \qquad (4)$$

$$\alpha(I) = 72.8I^3 - 42.88I^2 + 14.83I + 0.29 \qquad (5)$$

$$C_d(I) = -9.37I^4 + 10.22I^3 - 4.33I^2 + 0.89I + 0.02 \qquad (6)$$

Where I is the applied current (in amperes) to the MR-Damper. Based on experiments, the relations for C_d and α are obtained as functions of applied current. Also, $K_d = 0$ which indicates the effect of the position of the piston is appeared to be negligible in damping force.

2.4. Experimental Verification of Resistance Boundary Generation

To investigate resistance-boundaries generation using MR-Dampers, experimental and simulation analyses are conducted. To implement resistance boundaries, I developed an experimental prototype and a computer simulation environment using MATLAB/SimMechanics. Several resistance boundaries are first generated. I noticed that although participation of human operator is the right condition to establish real haptic operations, it will not give us enough resolutions to accurately control the experiment, identify the shape of the path and evaluate the quality of the performance. The other challenge was maintaining the same hand force while it moves along the resistance path. As a result, to have a better control over the situation and also to have consistency in simulations and experiments, hand motion is replaced by a linear motor.

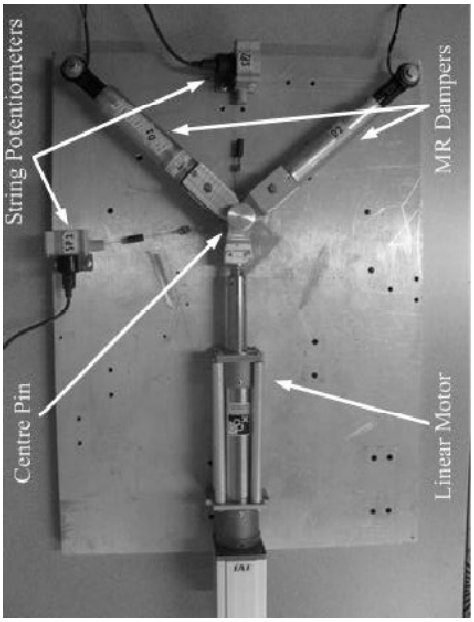

Figure 6: Experimental setup for testing the performance of resistance boundaries.

2.4.1. Experimental Prototype

To move the haptic platform a "ROBO Cylinder ERC" Series produced by IAI is used. This linear motor comes with software that enables the users to control velocity/acceleration of the extension/contraction of its rod. Linear motor and MR-Dampers are located on a fixed isosceles triangular base. Two string potentiometers are used for finding the location of the centre pin. A schematic view of system is depicted in Figure 6. In order to avoid effects of unwanted torque in rotations, only revolute joints are used to connect the linear motor and MR-Dampers to ground as well as to connect them together at a centre pin (end-effector point).

Resistance boundaries are defined as function and generated by MATLAB as,

$$x_{de} = F(y_{ex}) \qquad (7)$$

Where x_{de} and y_{ex} are the Cartesian coordinates of the resistance boundary and subscripts de and ex refer to desire and experiment respectively. The goal in here is to monitor motor motion and guide it to move along the boundary. As motor moves, string potentiometers measure the exact location of the centre pin, i.e. x_{ex} and y_{ex}. Substituting y_{ex} in Equation (7) should make x_{de} and x_{ex} the same, only if the motor centre pin (end-effector) moves exactly on the resistance-boundary. The difference between x_{ex} and x_{de} indicates where the centre pin is located with respect to the resistance-boundary. For instance, the positive difference means that the centre pin is in the right side of the actual resistance boundary. In our experiments, the linear motor is programmed to push the center pin upward. Therefore, to guide back the motor to the resistance boundary, the controller should activate the right hand side MR-Damper to stop the centre pin moving in that direction. This is done by applying a current, proportional to the $|x_{ex} - x_{de}|$ to the right damper. This controlling strategy is effective, straightforward, and easy to implement. All these calculations will be performed by the controller. The controller uses a PID controller for commanding the MR-Dampers. The block diagram of this control strategy is depicted in Figure 7.

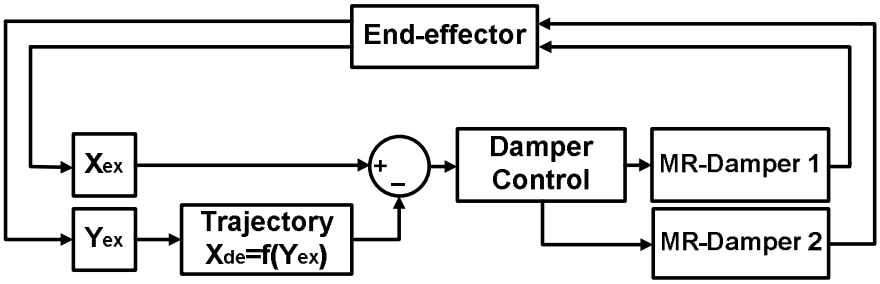

Figure 7: Feedback PID control block diagram.

2.4.2. SimMechanics Simulation

A simulation platform has also been developed using MATLAB/SimMechanics to investigate the validity of the MR-Damper model in predicting the motion of the end-effector in the resistance map. SimMechanics is a useful toolbox which facilitates modeling kinematics and dynamics of three-dimensional mechanical systems. This toolbox has been adopted as a powerful simulation tool in many research applications such as rehabilitations [59], robotics [60, 61], path planning [62] and human motion simulations [63]. SimMechanics enables us to build a model without deriving and programming dynamic equations of motions. Using this tool, I have effectively model the linear motor and MR-Dampers bodies and the joints according to the platform shown in Figure 6. All joints are assumed to be frictionless. Masses and inertias of MR-Dampers and motor are also included in the model. To simulate the developed SimMechanics model, it is loaded into Simulink environment. Figure 8 presents the main window of Simulink environment. As seen in the simulator, a feedback PID controller is designed to control the linear motor force to the centre pin so that the velocity of the motor remains constant throughout the simulations. At every instant, the location of center pin is fed back to the system controller. Based on the programmed resistance map, controller determines the magnitude of the currents that needs to be applied to each damper. A subsystem is also provided for Bouc-Wen MR-Damper model, which is developed in section 2.3, to calculate resistance forces as a function of input currents, and MR-Damper velocities. MR-Dampers have a maximum continues working current of 1 ampere. In order to consider this issue, in simulations, saturation blocks are used to ensure that applied currents to the MR-Dampers are below maximum allowable value at all times.

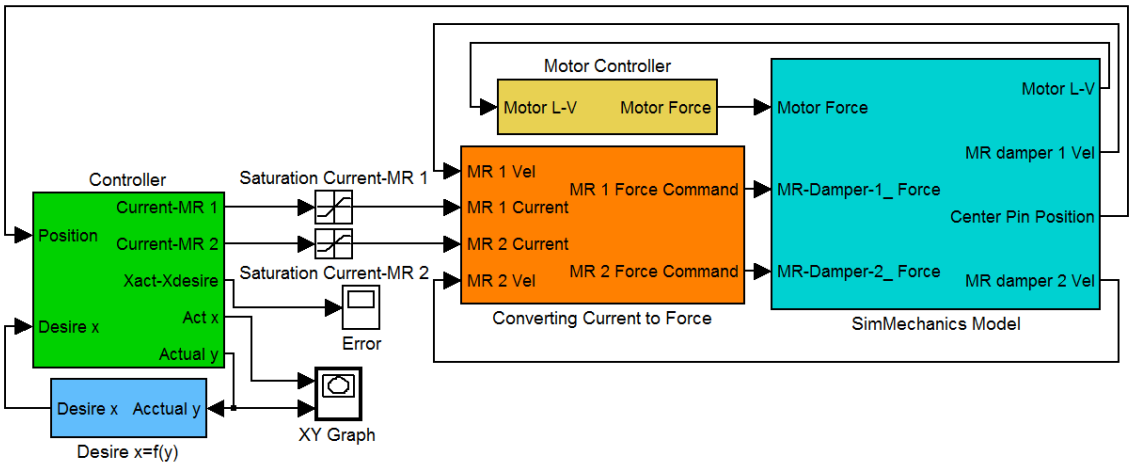

Figure 8: MR-Damper based haptic interface simulation using SimMechanics.

The same test paths are used for both simulation and experiments and results are depicted in Figure 9. These results indicate that MR-Dampers are capable of generating resistance boundaries.

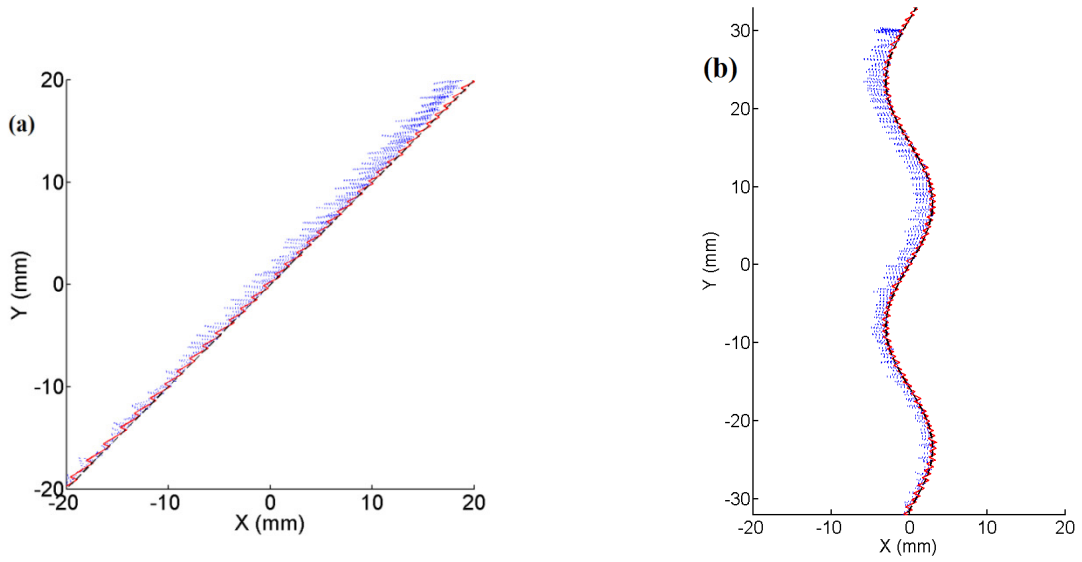

Figure 9: Comparison of the test results with predicted results, a.(line) X vs. Y, b.(sinusoidal) X vs. Y, ... experimental data,____ simulation result,, ----- resistance-path.

As seen in the previous results, resistance-boundaries are successfully generated by employing two MR-Dampers. In the next step, the idea of resistance

boundary is extended to generate resistance maps. To do this, I used the same simulation model developed for testing the resistance boundaries. The maps are generated by defining functions for each of the resistance boundaries. The test resistance maps are depicted in Figure 10.

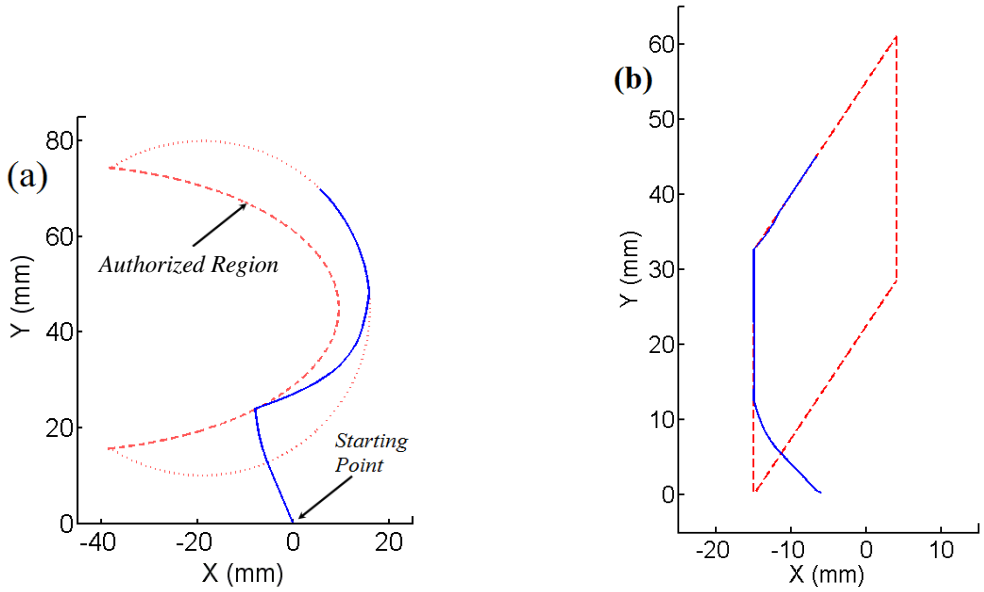

Figure 10: Centre pin position control inside an authorized region, a. First case b. Second case.

In these maps, authorized regions are defined inside a boundary that is determined by two intersecting functions $x_l = f_1(y)$ and $x_r = f_2(y)$ (subscript l and r stands for the left and right). During the operation, centre pin's position is monitored. As long as the centre pin is in the authorized region ($f_1(y) \leq x \leq f_2(y)$), the MR-Dampers are inactive, however, as soon as the centre pin reaches the resistance borders, a signal will be sent by the controller and MR-Dampers will be activated based on centre pin's position inside the map. For example, if user pushes the end-effector to the right side of the authorized region (where $x \geq f_2(y)$) the controller receives a positive position error and then activates the right side MR-Damper to resist the motion in that direction. As result, the centre pin position is maintained inside the authorized region. Figure 11 shows the general architecture of the proposed control system.

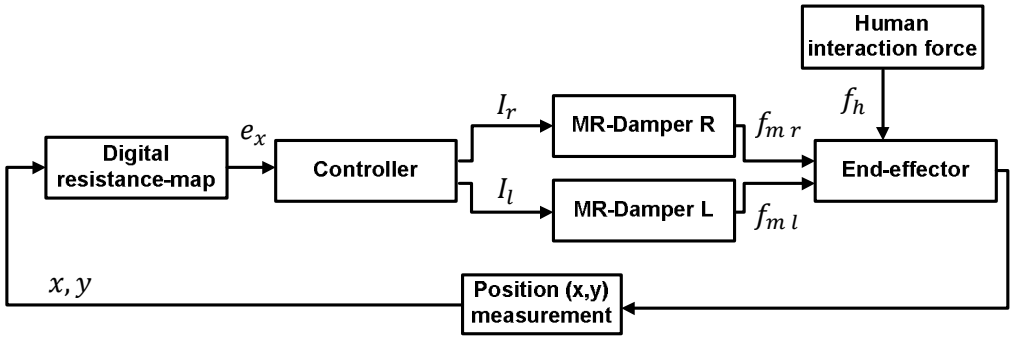

Figure 11: Control system architecture for resistance map generation of a 2_D system.

2.4.3. Guiding Path to the Authorized Region

Another important issue to be considered in designing the controller is the potential of the centre pin to be located outside of the authorized region either by pushing it so hard to the other region or starting the motion from a location other than authorized region. In these cases the user will be trapped in a high resistance region. To help users, two approaches can be undertaken. In the first approach, controller re-originates the coordinates to relocate the authorized region position inside the digital resistance-map so that end-effector falls again inside the authorized region. This approach is easy to carry out; however, it might not be always a feasible approach. The major drawback might be that the authorized region completely or partly located outside of the platform workspace. In the second approach, user will be guided to find a path to the authorized region. In this case, the controller is designed to offer a guide path by easing the resistance in a certain direction that if it will be followed, the centre pin will be directed into authorized region. The procedure of producing guiding paths is automatic and regenerated dynamically fast enough to ensure that users will not lose it. This concept is demonstrated in Figure 10. In these simulations the initial centre pin position is set outside the authorized region. According to the results, the centre pin could find the path to the authorized region. This has also been shown by performing experiments using a point outside the resistance path. The experimental results in Figure 12 also demonstrate the effectiveness of the strategy.

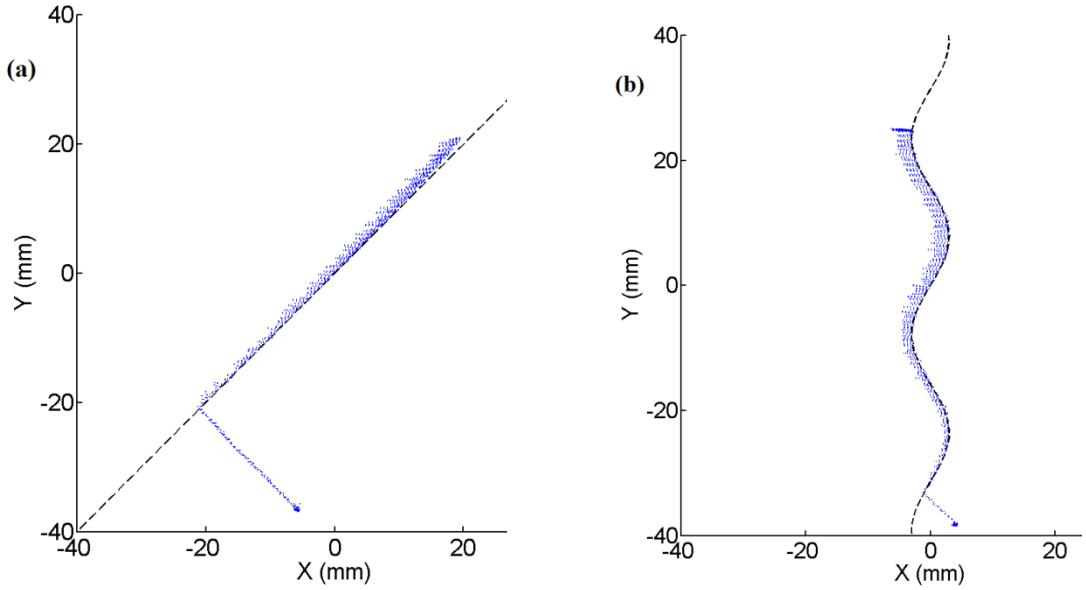

Figure 12: Experimental test for demonstration of path finding for initially being set out of resistance path, a. First path b. Second path,,.....experimental result, ------resistance paths.

2.5. Digital Resistance Map Generation Using SimMechanics Simulations

To further investigation of the effectiveness of the proposed haptic platform and the DRM methodology, I performed a new series of simulations to monitor its ability in generating the prescribed digital resistance maps across the interface workspace. 1-D, 2-D and 3-D models of haptic platforms are simulated using MATLAB/SimMechanics. In the simulations, human interaction with the platform is replaced by an external force (f_h) applied to the end-effector. The Interface's end-effector is initially located inside the authorized region and is then pushed by the external force to outside of the authorized region at different directions. The amount of external forces needed to overcome the resistance and move the end-effector to the prohibited regions are monitored for each location inside the workspace.

2.5.1. 1-D Digital Resistance Map Generation

To better explain the concept of resistance map generation the simple 1-D case is studied first. To generate 1-D resistance map only one MR-Damper is needed as shown in Figure 13. Here workspace is a line and the end-effector position is defined by a single variable x. As an example, the permissible range of motion is selected between $x = -4\ mm$ and $x = 5\ mm$, and other locations along the x axis are treated as prohibited regions. The amount of resistive force at each location on the prohibited area (resistance region) is determined to be proportional to the distance of end-effector from the permissible region. It should be mentioned that such assignment of the resistance force (proportional to distance) to the locations is not unique and can be set to any desired scheme. In order to study effectiveness of the resistance map methodology, a simulation is conducted using SimMechanics with the setup shown in Figure 13.

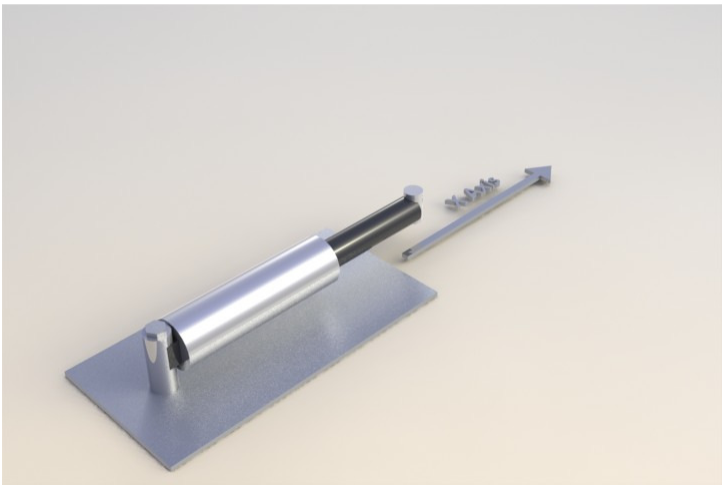

Figure 13: A schematic view of 1-D platform.

The block diagram of the controller which implements the methodology is presented in Figure 14. To generate the resistance map the position of the end-effector (x) is monitored and compared with the predefined digital resistance map. As long as the end-effector is inside the authorized region ($-4 \leq x \leq 5$) MR-Damper remains inactive, however, as it approaches the upper or lower limits, controller starts applying current (I) to the MR-Damper and as result, resistive force is generated based on the magnitude of position error (e_x).

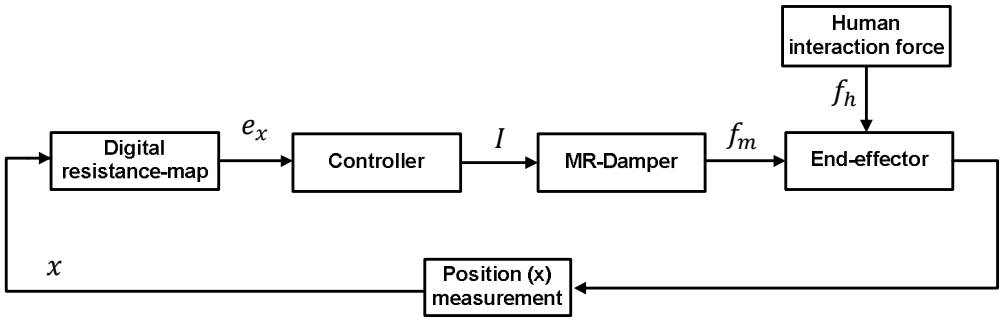

Figure 14: 1-D system block diagram.

The amount of external force needed to overcome the resistance and move the end-effector is shown in Figure 15 using color coded (intensity increase from dark blue to dark red). As it can be seen, no resistance is generated inside the authorized region (blue part) and hence patient can move the end-effector freely whereas resistive force increase as patient tries to move end-effector out of the region.

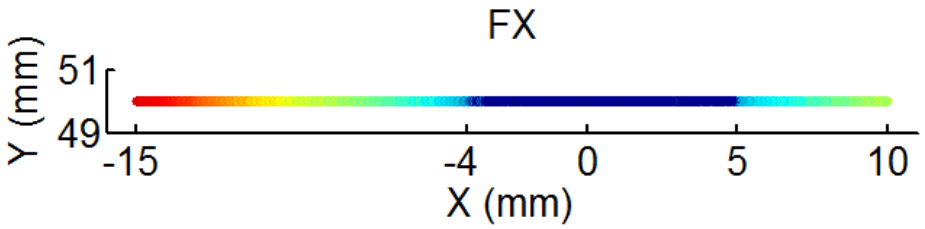

Figure 15: External force (F_x) applied to end-effector thorough the 1-D Resistance Map.

Another possible configuration for 1-D platform is employing a rotary MR-Damper instead of linear one where the resistance map will be defined as arcs on a circle of constant radius. In the following section 2-D digital resistance map generation is discussed which is the extension of 1-D resistance map.

2.5.2. 2-D Digital Resistance Map Generation

In the 2-D case we are dealing with a planar workspace and therefore at least two MR-Dampers are needed to cover the whole workspace. Figure 16 presents the 2-D platform where two linear MR-Dampers are employed in a parallel configuration.

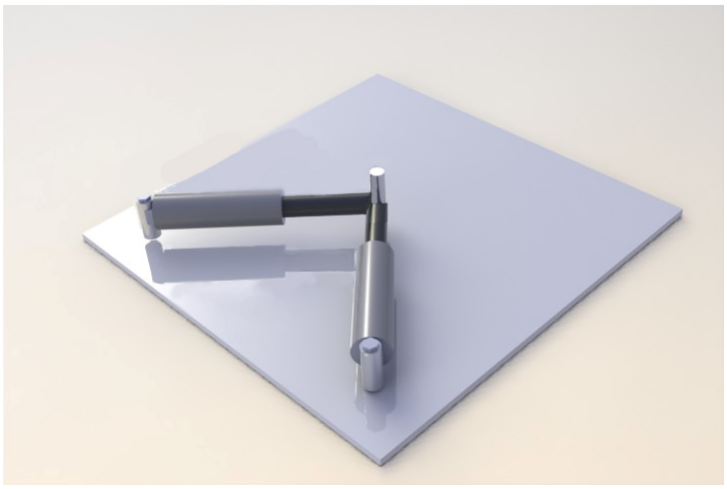

Figure 16: A schematic view of 2-D platform.

The challenging part of a 2-D system, Comparing to 1-D platform, is the control strategy. It is mainly because the controller must determine both the activation of the MR-Dampers as well as adjusting their input currents. The 2-D digital resistance map generation system is simulated for two different digital resistance maps. The selected maps are shown in Figures 17 and 19. Resistance boundaries are defined by two intersecting functions $x_1 = f_1(y)$ and $x_2 = f_2(y)$. An external force, similar to the 1-D design, is programmed to be applied at the end-effector point to move it inside the workspace. At each instant, the location of the end-effector (x, y) is monitored and matched with the resistance map to determine if the motion is inside the authorized region $(f_1(y) \leq x \leq f_2(y))$, otherwise the controller sends appropriate command signals for the MR-Dampers.

Figures 17-20 illustrate, components of the external forces acting on the end-effector to move it thorough the workspaces. The magnitudes of the forces are represented by color codes with the dark red indicating the highest intensity. Authorized regions are almost clearly distinguishable from the rest of the maps by colors (dark blue parts).

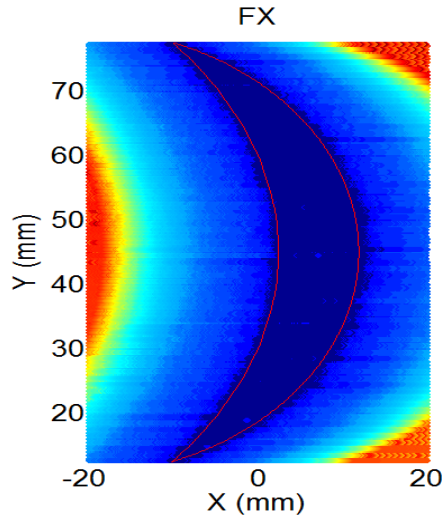

Figure 17: External force (F_x) applied to end-effector thorough the 2-D resistance map (1).

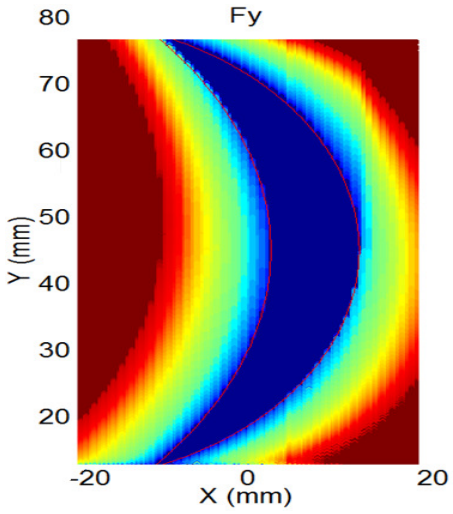

Figure 18: External force (F_y) applied to end-effector thorough the 2-D resistance map (1).

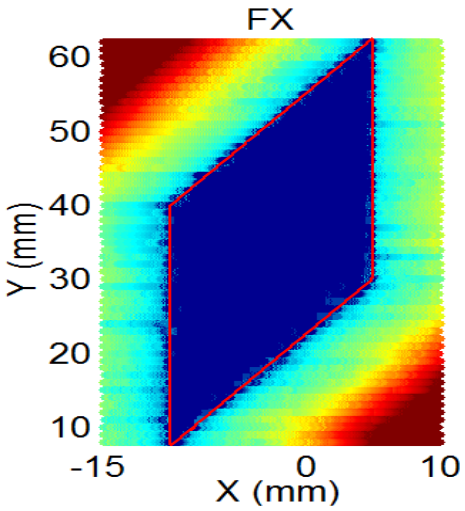

Figure 19: External force (F_x) applied to end-effector thorough the 2-D resistance map (2).

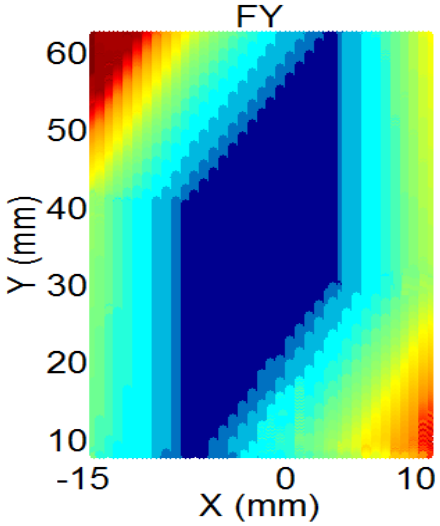

Figure 20: External force (F_y) applied to end-effector thorough the 2-D resistance map (2).

As expected, larger forces are required as the end-effector approaches locations farther from the authorized region (red parts). In rehabilitation device it is assumed that

patient would sense the increase of resistance to the motion as the end-effector is pushed outside of the authorized region and hence selectively correct the motion and get back to the authorized region. These results confirm the success of the system in implementing digital resistance map methodology.

2.5.3. 3-D Digital Resistance Map Generation

The idea of generation of resistance map can be extended to 3-D platforms as well. A potential design of such platform can be obtained by adding a third linear MR-Damper normal to the platform plane earlier proposed for the 2-D . As shown in Figure 21, MR-Dampers are attached to the ground thorough universal joints from one end and the other two dampers on the other end. The platform is modeled using SimMechanics and for simplicity the effects of gravity is neglected.

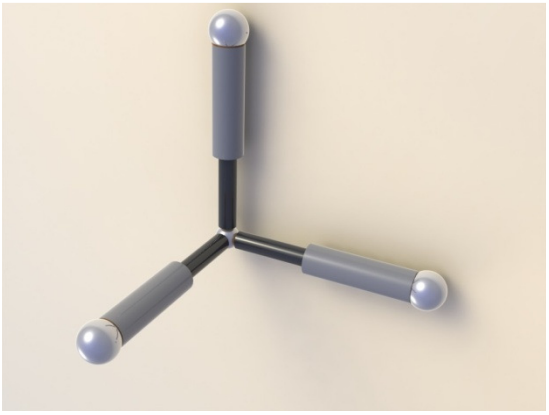

Figure 21: A schematic view of 3-D platform.

For the simulations the authorized region is set as a sphere and the end-effector is pushed from the sphere center to the outside of the authorized region at different directions. Total applied external force at the end-effector indicates the magnitude of resistive force to motion at different locations. For simplicity and clarity, the simulation results are plotted only for first quarter of the 3-D workspace (Figure 22).

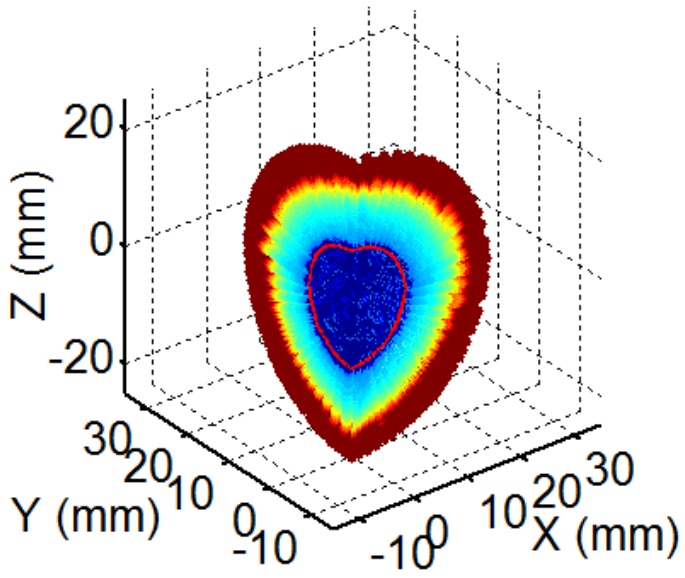

Figure 22: Total External force (F_t) applied to end-effector thorough the 3-D resistance-map.

Similar to 1-D and 2-D systems, the DRM has successfully deactivated MR-Dampers inside the authorized region and generated resistance to motion at other locations.

In Figures 15, 17-20 and 22 in all directions from one point forward, the magnitude of external force that is needed to move the end-effector, remains constantly at a fixed high level (dark red parts). This is because of the saturation blocks I used in the simulations to keep the applied currents to the Dampers below 1 ampere.

As explained in section 2.4.3, an issue that needs to be addressed is the possibility of trapping inside the prohibited areas by pushing end-effector too hard or by starting the exercise from a point outside the authorized region. To overcome this problem, the controller is programmed to monitor end-effector motion and detect the trapped situations. The controller will then determine a path and remove the resistance along it to help the user return to authorized region. To simulate the situation, the end-effector has initially located at a position outside the authorized region. As it is simulated in Figure 23 the controller has guided the user by easing the resistance in a direction toward the authorized region. This means that, although the end-effector is inside the

resistance region, user can follow the guiding path to avoid high resistance on the way back to the authorized region.

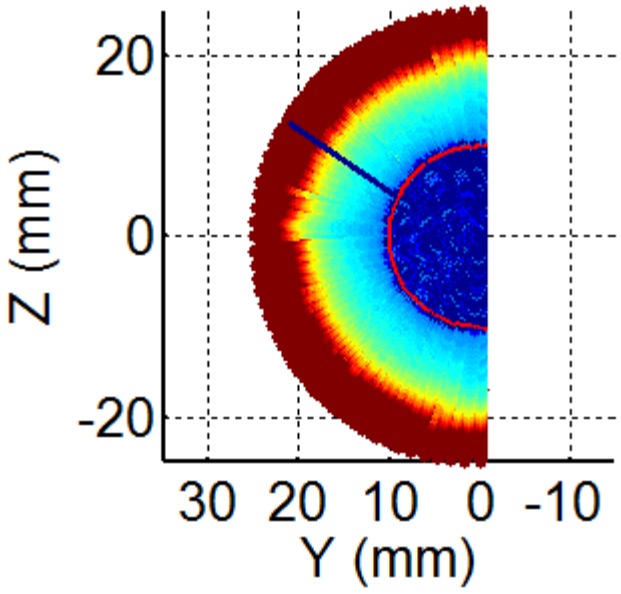

Figure 23: Simulation results (total external force) for system being set initially outside authorized region.

2.6. Conclusion

In this chapter, the design and development of a novel haptic interface for rehabilitation application is presented. This system is developed by generating a resistance map in a workspace to control and constrain patient's muscle movement. Linear MR-Dampers are used to create the resistance maps. MR-Dampers are modeled using Bouc-Wen model. The parameters of the mathematical equation of the MR-Damper are identified experimentally. To test the performance of the proposed system, resistance boundaries are generated and verified experimentally. A simulation environment is also developed using MATLAB/SimMechanics. The simulation and experimental results are compared and a close agreement is observed. Finally different resistance maps are generated and the control strategy is implemented by performing simulations. The controller of the haptic system is also designed to help the users find the path if they are trapped inside a wrong region. This feature is also simulated and

verified experimentally. The proposed system will bring flexibility in trainings damaged muscles. Also, the device is safe and unlike those actuated by motors, there is no risk of damaging muscles by creating unwanted forces. Due to its compactness and affordable price, the MR-Damper base rehabilitation haptic interface can also help patients to do their exercises at home. The device can record the motions during the exercise and send them to physiotherapists where they can easily monitor the performance of patients and reprogram the device for new exercises. This tool also will be very useful in improving rural health where family physiotherapists and other clinical resources are scarce.

3. Development and Investigation of a Semi-Active Polar Planar Haptic Interface Using Digital Resistance Map Concept

In spite of the promising results reported in chapter 2, lack of information about user's input force is an unsolved issue that affects the efficiency of the proposed haptic interface and Digital Resistance Map (DRM). In chapter 2, desired resistance forces are determined only based on end-effector position. For every location in the prohibited region, the deviation from the authorized region is calculated and proportional to that, electrical currents are applied to MR-Dampers. This control strategy is straightforward and easy to implement, however, it suffers from two drawbacks. First, the proposed DRM, is unable to detect the direction of user force. Therefore, it applies the same magnitude of resistance to the end-effector for all the directions. Second, The DRM regulates the applied currents to the MR-Dampers using a non-feedback controller and therefore, due to non linear characteristics of MR-Dampers, it is difficult for the proposed DRM to properly control the magnitude of generated resistance.

A possible solution for the mentioned drawbacks is to include user force information in the controller. User force information helps the DRM to detect users force direction and change the magnitude of resistance in different directions. This enhances users' ability to find their path to return to authorized regions. User force information also enables the DRM to provide higher resistance force resolution through a force feedback controller. In this chapter, the DRM is modified to include user force information in computations. The DRM is expanded and introduced as a new display rendering algorithm (DRA) for semi-active haptic interfaces. To implement the enhanced DRM, an experimental polar semi-active haptic interface is designed and fabricated using a rotary and a linear MR-Dampers. This haptic interface is equipped with a force sensor to measure magnitude and direction of users' input force. To verify the effectiveness of the enhanced DRM and new haptic platform, in computing and generating haptic scenes, several experiments are carried out and the results are presented.

3.1. Haptic Rendering Algorithm Using Digital Resistance Map Concept

In this section, I expand the DRM and introduce it as a haptic rendering algorithm for semi-active haptic interfaces. Typically, haptic rendering algorithms involve two processes (1) synchronizing, and (2) force feedback. A virtual reality is first synchronized with a platform workspace such that as the platform end-effector moves inside the workspace, its corresponding point in the virtual environment also relocates. The motion of the point that represents the end-effector is then used to compute the interaction force with the virtual environment. Finally, this force is reproduced by the workspace actuators to represent features of the virtual environment.

In haptic rendering algorithms, a virtual environment contains obstacle regions where penetration inside them is prohibited. The main objective of the DRM methodology is to discriminate prohibited and authorized regions by generating distinct resistance force against motion. In the enhanced edition of DRM methodology, in addition to the location of the end-effector, I also used direction of the user input force to determine the resistance forces that is needed to be generated at each time. By improving the logical patterns of generated resistive forces in the enhanced DRM, I try to instruct operators to more easily find their location relative to the resistance boundaries and return to authorized regions. Figure 24 illustrates an enhanced version of the Resistance Map that was described in section 2.2. In this new map, the lines inside resistance region represent the intensity/direction of the maximum resistance. The magnitude of the resistance at each point is determined using end-effector distance from the resistance boundaries and its direction of motion. The resistance patterns in the left side of the graph show the resistance intensity/direction of the map for two arbitrary points outside the authorized region. For example, if the end-effector is moved from point 1 to 2, maximum resistance will be applied and the resistance will increase by moving further away toward point 3. In reality, the strategy for assigning resistance in DRM is not unique and can be planned based on the application to improve the accuracy and effectiveness of the interaction with operators. One potential scenario is increasing the force proportional to the distance of the end-effector from the resistance boundary. The proportionality of the resistance can help operators to guess end-effector's distance from the resistance boundaries. The other factor which can be

considered in the resistive force generation strategy is the direction of user input force to move the end-effector. One scenario might be reducing the resistance if the end-effector is pushed in the direction that takes it back to the authorized region. For example, if the end-effector is moved from point 3 to 1, the resistance to the motion can be set to zero, although the end-effector is located outside the resistance-boundary. The directionality of the resistance can be programmed properly to help operators in finding the shortest returning path to authorized regions. The other advantage of this approach is preventing operators from getting trapped inside the resistance region. Using the proportionality and directionality approaches is a more comprehensive way to have an effective interaction with operators.

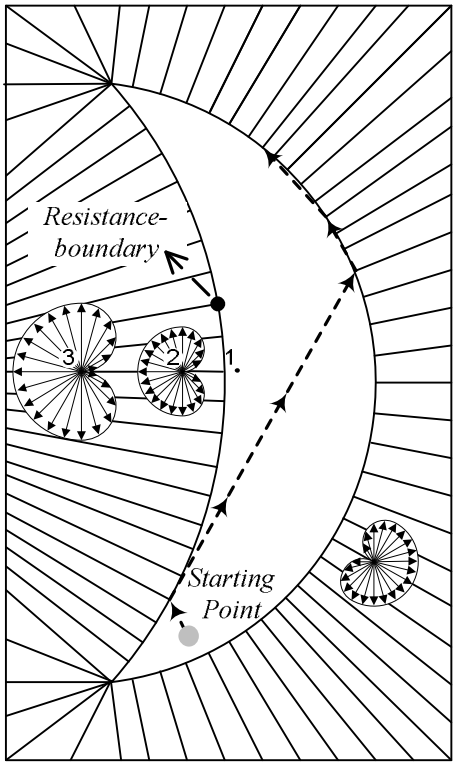

Figure 24: A schematic view of Resistance Map and resistance boundaries (enhanced version).

3.1.1. Dynamic Resistance Maps

A DRM does not necessarily need to be static and fixed and can be programmed to change dynamically. One potential scenario is implementing multiple layers of virtual

maps with distinct resistance patterns for the same workspace. These maps can be activated (one at a time) once their corresponding conditions are met. Figure 25 is an example where a desired trajectory starts from point A and subsequently proceeds to points B, C, D, E, B, and F. This trajectory crosses itself at point B, thus with a static Resistance Map (Figure 25 (a)); operator may have several choice to follow, i.e. ABCDEBA, ABEDCBA, ABEDCBF, or be trapped in the loop BCDEB.

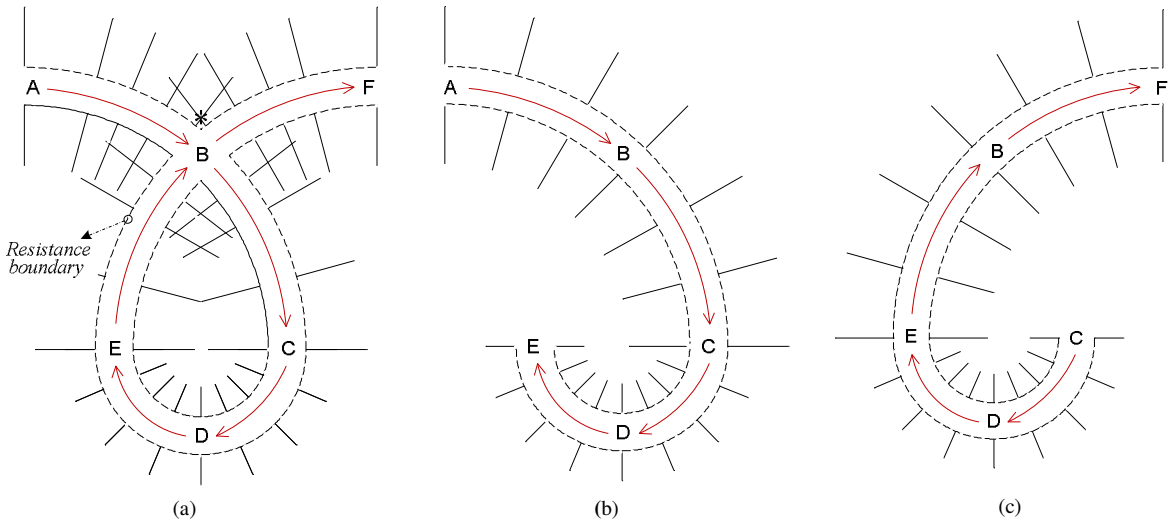

Figure 25: A schematic view of dynamic resistance map; dash line shows the Resistance boundary between resistance-free trajectory and resistance regions; solid lines show the resistance directions inside resistance regions; red arrows shows the planned motion of end-effector in resistance-free trajectory; the asterisk (*) in left figure shows a point, as an example, with conflicted resistance patterns.

The other shortcoming of static Resistance-Map is the conflicted resistance patterns of regions in the vicinity of the crossing point B. Thus, for the point shown by "*", which has the same distance to both right and left sides of the free resistance trajectory, there is uncertainty for guiding the motion. Here, the dynamic Resistance-Map can address the problem by introducing two maps (Figure. 25 (b) and (c)). The first map will be activated when the end-effector has not been passed through D, and the second map will be activated when this condition is met.

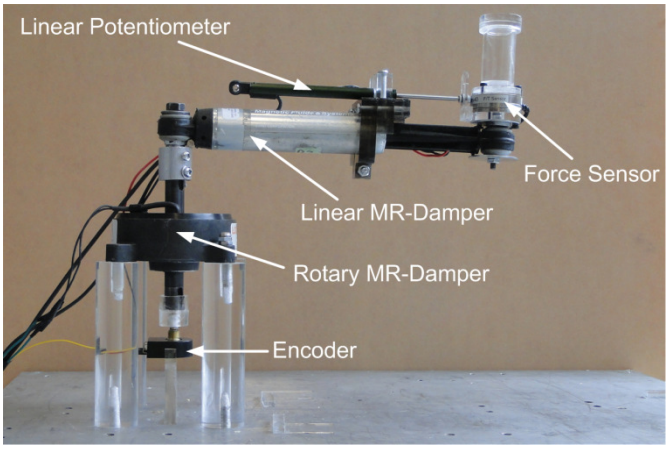

(a)

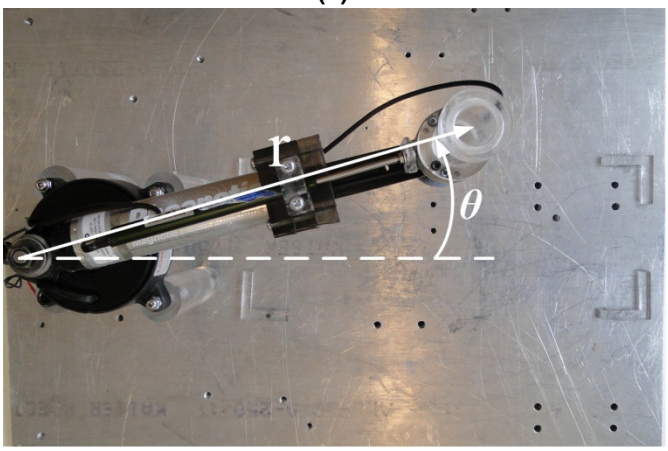

(b)

Figure 26: Haptic display platform; (a) side view, (b) top view.

3.2. Experimental Platform

To implement the enhanced DRM in a 2-DOF haptic interface, a linear and a rotary MR-Damper as shown in Figure 26 are employed. In this design the rotary damper is fixed to the base and the linear damper is attached to it. The combination of a linear and rotary MR-Dampers enables the interface to generate planar resistive forces. To identify location of end-effector the rotary MR-Damper is coupled with a quadrature optical encoder with 4000 counts per revolution and a Celesco MLP-75 linear

potentiometer is used to measure the displacement of the linear MR-Damper. A Mini 40 ATI 6-DOF load cell is mounted at the end-effector to sense operator's input forces. A PWM amplifier (16A20AC-Model) from Advance Motion Control is used to power the MR-Dampers. The PWM amplifiers are set in current mode to decrease the response time of the MR damper's magnetic circuit [53]. A Sensoray 626 PCI DAQ is used to interface the hardware with the controller.

3.3. Rotary MR-Damper Modeling

I have previously presented (section 2.3) a mathematical model of the linear MR-Damper. Similarly, this section, models the rotary MR-Damper based on Bouc-Wen model. The rotary MR-Damper is RD-2087-01 Rotary Brake made by Lord Co. The MR-damper specification is summarized in Table 2.

Table 2: Rotary MR-Damper specification

Input Current, Amp	Operating Speed, rpm	Torque @ 1A, Nm (lb ft)	Operating Temperature, °C (°F)
1.5 max	120 max	4 (2.95)	-35 to +60 (-31 to +140)

An experimental setup as shown in Figure 27 is built to determine the Bouc-Wen model parameters for the rotary MR-Damper. A DC motor is used to excite the MR-Damper and a T8-2-A7A torque transducer and an encoder are employed to measure torque and rotation angle. Sensors are interfaced with MATLAB/Simulink by Sensory 626 DAQ. Using a PID feedback controller, the DC motor is commanded to apply sinusoidal excitations to the MR-Damper with frequency from 0.2 to 0.4 Hz and amplitude from 2π to 4π radians. For each frequency-amplitude excitation pairs, MR-Damper is tested under the applied current varying from 0.50 to 0.75 A in increments of 0.05 A.

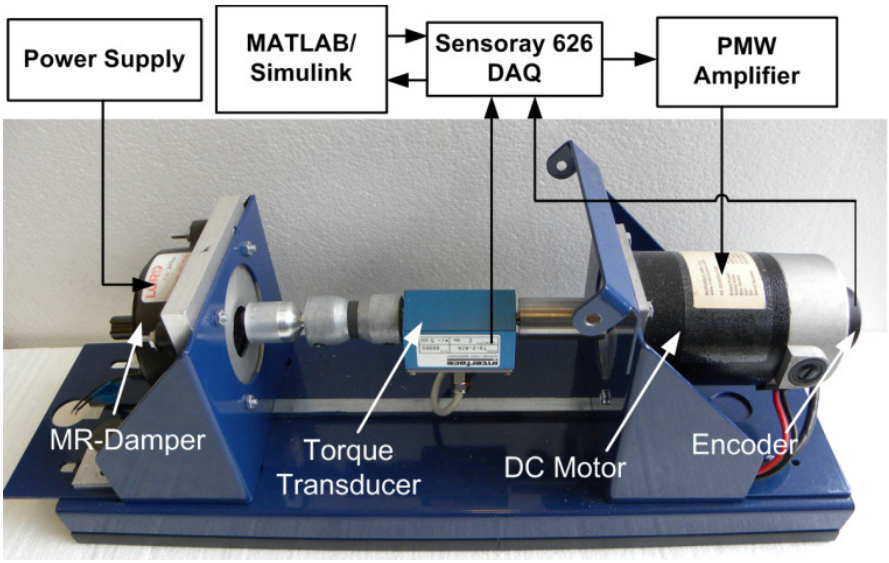

Figure 27: Experimental setup for rotary MR-Damper modeling.

The damper stiffness coefficient K_d represents the effect of air spring, which does not exist in the rotary MR-Damper; therefore, it is set at zero. The Bouc–Wen model parameters are,

$$[K_d, A, \gamma, n, \beta] = [0, 2.7789, 5.1269, 1, 1.5960\ ] \qquad (8)$$

$$\alpha(I) = -0.208I^3 + 0.377I^2 - 0.215I + 0.042 \qquad (9)$$

$$C_d(I) = -25.99I^3 + 49.02I^2 + 28.05I + 5.23 \qquad (10)$$

An example of comparison between the experimental data and model-predicted values are shown in Figure 28.

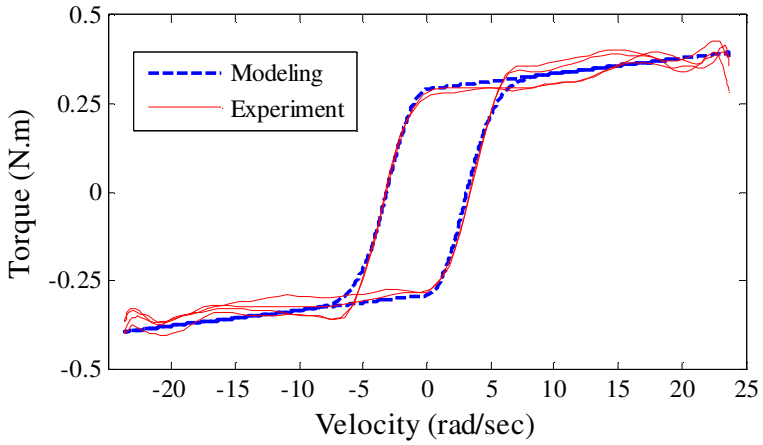

Figure 28: Comparison of experimental results with model-predicted results.

3.4. Haptic Interface Control Structure

A schematic view of the haptic interface is shown in Figure 29. In this system, the end-effector position and operator's input force are measured and fed to the control module.

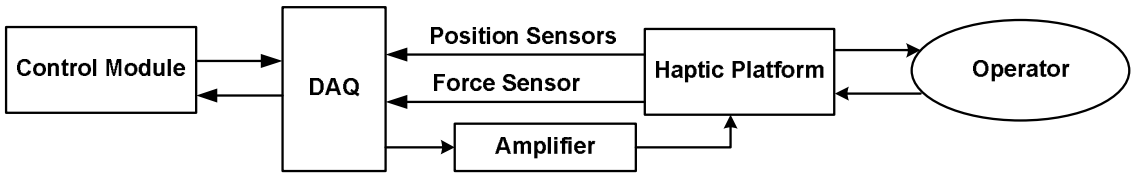

Figure 29: A schematic view of haptic interface.

The controller is developed in MATLAB/Simulink environment and its schematic is depicted in Figure 30. Using the sensors data and based on the programmed Resistance-Map, the controller determines the magnitude of the electrical current that is required to be applied to the MR-Dampers.

In this control system, virtual environments are programmed in the Digital Resistance Map section. This section is responsible for computing the magnitude and direction of the resistive forces that are needed to be generated by the actuators. The force computation process is performed in two steps. In the first step, it is assumed that

the end-effector is moving along the maximum resistance directions shown in Figure 24 and accordingly the maximum possible resistive force is calculated. Then, the magnitude is corrected based on the actual direction of the motion with a gain coefficient between 0 and 1. These steps will be explained in details in sections 3.4.1 and 3.4.2. Force vectors are then sent to the feedback force controller to calculate the proper electric currents for the MR-Dampers and generate the required resistance to the motion. The calculated currents are checked with saturation blocks and commands are sent to the dampers PMW amplifiers.

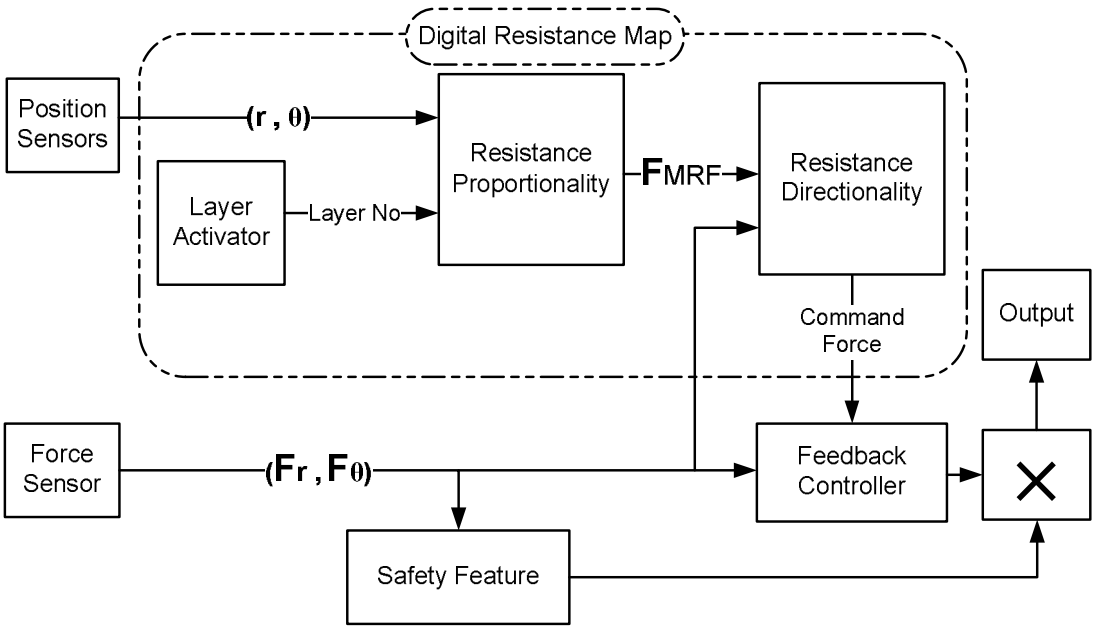

Figure 30: A schematic view of the controller.

The controller is also programmed with a Layer-Activator block to handle dynamic Resistance-Maps. Dynamic maps as explained in section 3.1.1 are comprised of multiple layers of static DRMs. These layers are needed to be activated upon certain events are met e.g. entering a region in workspace, passing a point, etc. To implement this, all layers are first programmed in the Digital Resistance Map section and the Layer-Activator block switches them by keeping the history record of the end-effector position and checking the conditions for different events.

Another important subject to be considered is preventing potential damages to the sensors during the operation. This is mainly to protect the force sensor from potential

damages due to excessive operators' force. This issue has been addressed by adding a safety feature to the controller which deactivates the MR-Damper and stops the experiments upon receiving excessive force.

3.4.1. Resistance Proportionality

Resistance Proportionality block is responsible to calculate the maximum resistive force vector ($\boldsymbol{F}_{MRF}$) for each point inside the Resistance Map. The direction of these force vectors are (along the lines shown in Figure 24) toward the authorized region, and their magnitudes are proportional to position error from the resistance boundary, represented by variable "Er". The positive Er indicates that the point is outside the resistance boundaries and the motion at that point needs to be corrected by applying resistive forces. A negative Er, however, confirms that the point is inside the authorized regions. Depending on the requirements of an application, an appropriate scenario can be selected for the proportionality of $\boldsymbol{F}_{MRF}$ magnitude to the position error. Figure 31 has depicted two possible proportionality scenarios. In the first scenario, called P1, the $\boldsymbol{F}_{MRF}$ magnitude is set to zero for negative errors. This means that the motion is not resisted inside the authorized region and operators can freely move the end-effector there. However, the motion is resisted in the regions where $Er > 0$.

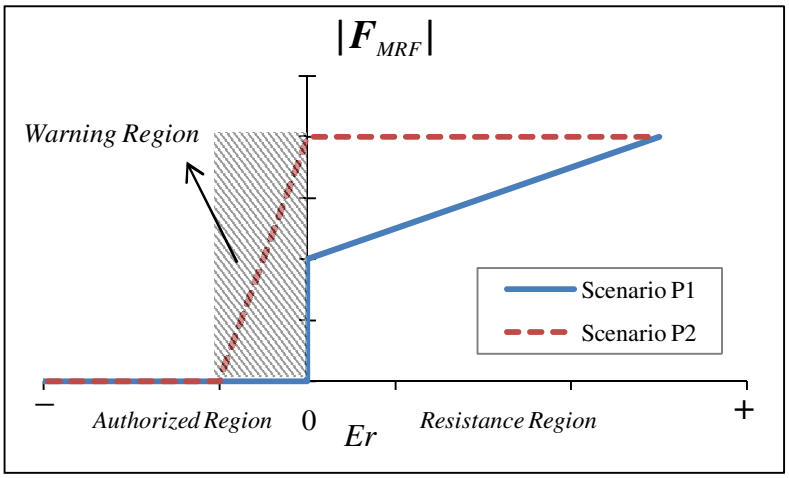

Figure 31: P_1 and P_2 resistance proportionality scenarios.

In the positive side of diagram, the $\boldsymbol{F}_{MRF}$ magnitude is defined as a linear function of error ($|\boldsymbol{F}_{MRF}| = a + b \times Er$). The offset a is used at $Er = 0$ to ensure that operators

will feel a sensible amount of resistance upon entering to the resistance region. In the second scenario, called P2, it is assumed that even a small penetration into the resistance region is prohibited. Surgical procedures are examples of this case where conducting operations on certain regions is not allowed. In P2, the resistive force will be applied and gradually increased from a close vicinity of the resistance boundaries to provide a force feedback warning for operators. The $\boldsymbol{F}_{MRF}$ magnitude increase can be proportional to the distance of the end-effector from the resistance boundary and maintained at its maximum in the entire resistance region.

3.4.2. Resistance Directionality

The Resistance Directionality block is in charge of correcting the maximum resistive force ($\boldsymbol{F}_{MRF}$) based on the direction of motion of the end-effector. The inputs to the block are applied force vector ($\boldsymbol{F}_a$) from the force sensor, and the computed $\boldsymbol{F}_{MRF}$ vector from the Resistance Proportionality block. The angle (σ) between these two vectors determines whether the end-effector is pushed toward or away from the authorized regions. Using this angle, a gain (between 1 and 0) is calculated and multiplied by $\boldsymbol{F}_{MRF}$ to obtain the output force vector ($\boldsymbol{F}_{out}$). Here, two potential directionality scenarios are implemented to calculate the gain.

In the first scenario, called D1, the components of $\boldsymbol{F}_{out}$ vector in r and θ directions, i.e. F_{out_r} and F_{out_θ}, are obtained separately [64]. The value of the gains and the output force vector ($\boldsymbol{F}_{out}$) are obtained by:

$$gain_r = \begin{cases} 1 & F_{MRF_r} \cdot F_{a_r} < 0 \\ 0 & F_{MRF_r} \cdot F_{a_r} \geq 0 \end{cases} \qquad (11)$$

$$gain_\theta = \begin{cases} 1 & F_{MRF_\theta} \cdot F_{a_\theta} < 0 \\ 0 & F_{MRF_\theta} \cdot F_{a_\theta} \geq 0 \end{cases} \qquad (12)$$

$$\boldsymbol{F}_{out} = F_{MRF_r} \cdot gain_r \cdot \boldsymbol{e}_r + F_{MRF_\theta} \cdot gain_\theta \cdot \boldsymbol{e}_\theta \qquad (13)$$

Then, the relative direction of $\boldsymbol{F}_{MRF}$ and the operator's applied forces in each r and θ directions, i.e. F_{MRF_r} and F_{a_r} for r direction, and F_{MRF_θ} and F_{a_θ} for θ direction, is obtained using inner product of the two vectors. A negative product ($F_{MRF_i}.F_{a_i} < 0$) means that the end-effector is moving away from the authorized region and thus the motion needs to be resisted ($gain_i = 1$). This method is simple and easy to implement; however, it provides no resistance for the all the motions in which $F_{MRF_i}.F_{a_i} < 0$. Therefore, the force feedback to operators will not be sufficient to find the returning path to authorized regions.

In the second scenario, called D2, a gain is calculated to scale the $\boldsymbol{F}_{MRF}$ vector. The value of the gain and the output force vector ($\boldsymbol{F}_{out}$) are obtained by:

$$\sigma = \cos^{-1}\left(\frac{\boldsymbol{F}_a \cdot \boldsymbol{F}_{MRF}}{|\boldsymbol{F}_a| \cdot |\boldsymbol{F}_{MRF}|}\right) \qquad (14)$$

$$Gain = \begin{cases} 1 & \frac{\pi}{2} \leq \sigma \leq \pi \\ \sin(\sigma) & 0 \leq \sigma < \frac{\pi}{2} \end{cases} \qquad (15)$$

$$\boldsymbol{F}_{out} = |\boldsymbol{F}_{MRF}| \cdot Gain \cdot \frac{\boldsymbol{F}_a}{|\boldsymbol{F}_a|} \qquad (16)$$

In D2, the resistance outside the authorized regions is set zero only if σ is zero which happens when the end-effector is being pushed back to the authorized region exactly along the line shown in Figure 24. Using D2, the operator will be able to correct the direction of the motion and find the shortest returning path to authorized regions.

3.5. Experiments and Results

The effectiveness of the haptic interface in implementing the enhanced DRM is investigated by conducting experimental analyses. To examine the proportionality and directionality concepts, the operator's actuation force on the end-effector is required to

be monitored in the workspace. For the reliability of the measurements it is essential that the motion of the end-effector be consistent and sudden and unnoticeable directional changes do not affect the assessments. Similar to section 2.4, this problem is addressed by utilizing a programmable IAI linear motor model RCP2-SA6C to simulate an operator's actuation force on the end-effector. This motor has sufficient power to overcome the generated resistances by the MR haptic interface, and has an internal controller that can provide constant velocity or acceleration. As depicted in Figure 32, the linear motor is mounted on a sliding table that allows us to accurately position it for each experiment. A revolute joint is used to connect the end-effector to the linear motor. This joint includes a ball bearing that is fixed to the motor from the outer ring and connected to the end-effector from the inner ring.

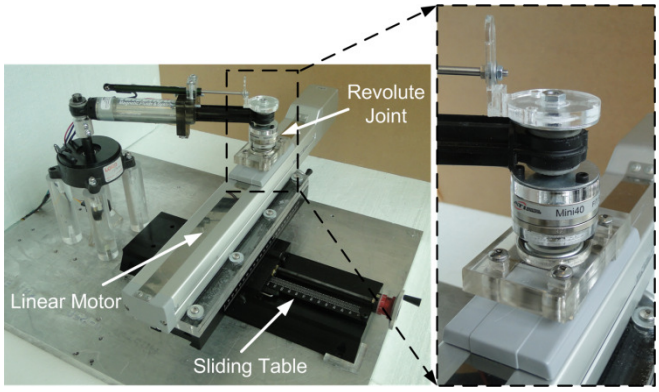

Figure 32: Modified platform for experimental tests.

Figure 33 shows the Resistance Map selected for the experiments. The end-effector is pushed horizontally to both left and right sides of the map and the input forces are recorded. Figure 33 and 34 show the results of experiments for P1 and P2 proportionality scenarios respectively. In these Figures the intensity of the force needed to overcome the resistance and move the end-effector is color coded (intensity increase from dark blue to dark red). As it can be seen in Figure 33, when the end-effector is in the authorized region, no resistance is applied to the end-effector; however, as it is reached to the resistance-boundary the motion is resisted. The gradual changes of colors from blue to red indicate that larger resistive forces are required to push the end-effector as it moves further away from the authorized region. In Figure 34, the motion starts from the middle part of the authorized region and MR-Dampers are activated at point "W", to notify the user about approaching the resistance regions. The amount of

the resistive force increases from zero at point "W" to the maximum value at the resistance boundary. It can be observed that the haptic interface is successful in deactivating and activating the MR-Dampers according to the programmed proportional scenario.

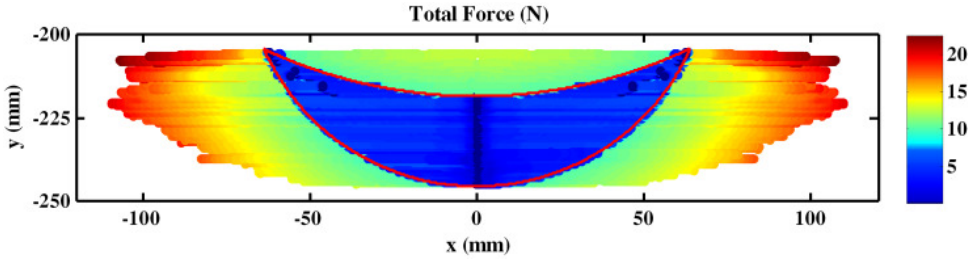

Figure 33: Experimental results for P_1 resistance proportionality scenario.

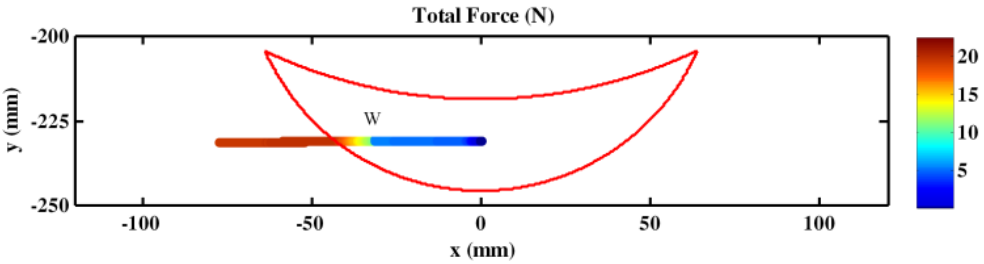

Figure 34: Experimental results for P_2 resistance proportionality scenario.

In order to illustrate the directionality concept, two experiments are conducted. For D1 the end-effector is initially placed in the middle of the map, then pushed forward outside the authorized region and finally pulled back to the initial position. As it can be seen from Figure 35, the MR-Dampers remain inactive until the end-effector reaches to the resistance-boundary. As the end-effector goes outside the boundary, the resistance increases and as soon as the direction of motion reverses, MR-Dampers become inactive to let the end-effector to be easily pulled back to the authorized region.

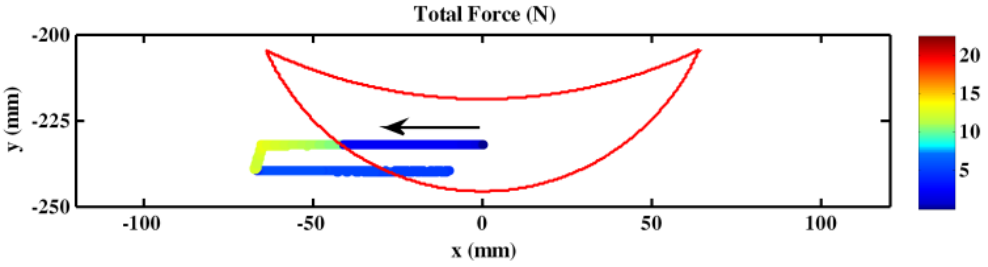

Figure 35: Experiment results for D_1 resistance directionality scenario.

To test D2, the end-effector is initially placed outside the authorized region and then it is moved in different directions. In Figure 36, the shortest path to the authorize region is vertically downward. Different magnitudes of resistive forces are applied depending on the direction of motion of the end-effector. The experimental results show that lower forces are required to move the end-effector toward the authorized region. This experiment demonstrates the effectiveness of the system in generating the directional resistance pattern described in D2.

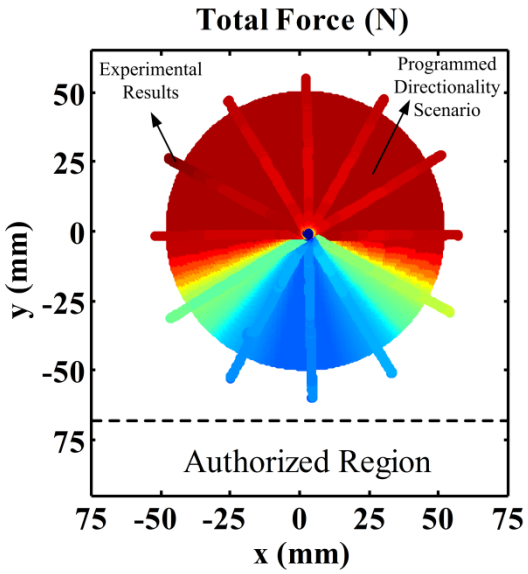

Figure 36: Experimental results for D_2 resistance directionality scenario.

Finally to evaluate the performance of the system in implementing Dynamic Resistance Maps, a two-layered Resistance Map similar to Figure 25 is generated. According to Figure 37, to complete the exercise as it is planned, the motion should start from point A and follow the trajectory to point F. At the beginning, the first layer (Figure 25 (a)) of the Resistance Map is activated. The second layer (Figure 25 (b)) is

activated when the end-effector passes point D. For the experiment, the end-effector is initially located at point 1 outside of the trajectory. Then it is pushed to the points 2,3,4,5, and 6 and finally is returned to the initial point thorough the same path. As it is shown in Figure 37, the patterns for the generated resistances are different for the forward (Figure 37(a)) and return (Figure 37 (b)) paths. This is because, in the forward path, MR-Dampers are energized by comparing the position and direction of the motion to the first layer, while, in the return path, they are energized by the second layer. This example shows that by activating one layer at a time, operators can be navigated through the correct trajectory.

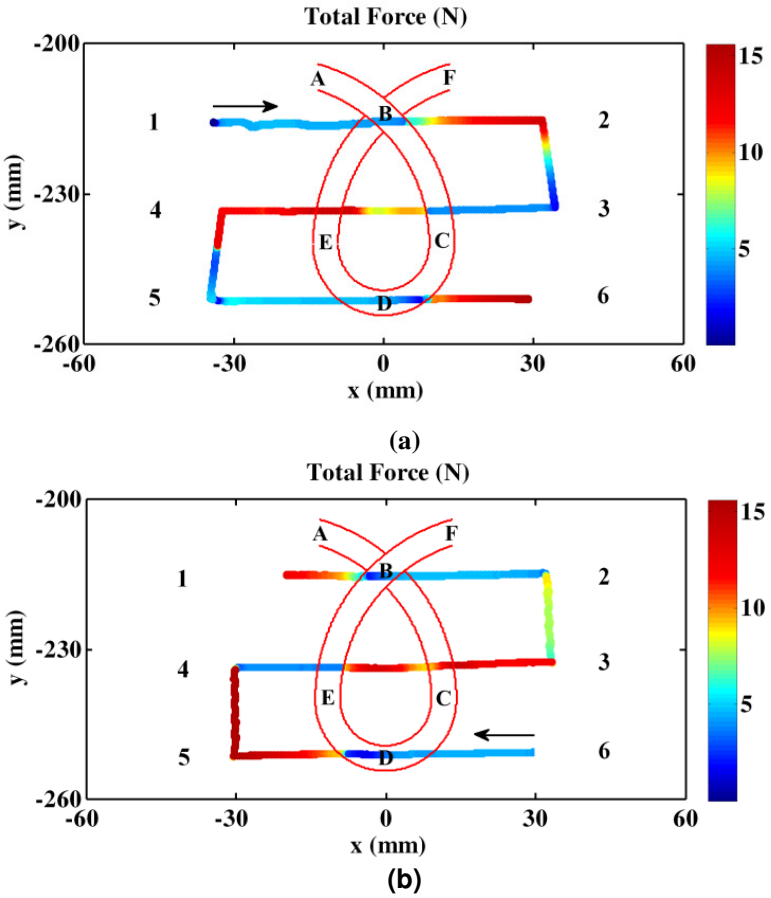

Figure 37: Experimental results for Dynamic Resistance Map; (a) forward path, (b) return path.

3.6. Conclusion

In this chapter, I built a new semi-active haptic interface using MR-Dampers and expand Digital Resistance Map concept, as a new haptic rendering algorithm, for implementation in our haptic interface. The DRM concept is an algorithm that is designed to use only resistive force for generating virtual environments. In order to effectively represent the elements of the virtual environment, the algorithm divides the workspace into regions with distinct patterns of resistances. To better navigate operator's motion, the position of the end-effector and its direction of motion are used to determine the magnitude of the resistance inside each region. The effectiveness of enhanced DRM is investigated by developing a new semi-active haptic interface. A linear and a rotary MR-Dampers are employed to produce resistance in a 2-DOF workspace. The rotary MR-Damper is modeled using Bouc-Wen model and the parameters of the mathematical equation are identified experimentally. Finally, different experiments are conducted to test and verify the performance of the proposed haptic system. The results indicate that the proposed rendering algorithm can be successfully implemented in haptic interfaces to allow operators to explore virtual environments. Moreover, this method is shown to be capable of handling dynamic virtual environments.

4. A Human Subject Study on the Effectiveness of Proposed System

The main advantage of the proposed haptic system to create a virtual environment is its ability to apply only resistive forces. Thus it is safe to be implemented for the applications such as rehabilitation that the safety of operators has outmost importance. The effectiveness of the haptic system is investigated in chapters 3, by replacing human interactions with a linear motor. This chapter, includes a human subject study to examine how the provided haptic feedback can effectively improve human explorations inside virtual environments. In this study, in addition to haptic, the participants are provided with visual feedbacks through a virtual reality. This study involves two tasks, each of which is performed by ten participants under different combination of haptic and visual feedbacks. In order to evaluate the utility of haptic feedbacks, statistical methods are exploited to analyze the participants' recorded data.

4.1. Integration of Haptic System with Virtual Reality

To incorporate and handle virtual models with Simulink program, MATLAB/Virtual Reality (VR) toolbox is used. This toolbox enables creating 3-D visual objects defined by Virtual Reality Modeling Language (VRML). VRML is a standard text format developed in 1994 for constructing and transmitting three-dimensional (3-D) virtual worlds.

Virtual objects are developed by SolidWorks and V·Realm™ Builder softwares and outputted as standard VRML format (*.wrl). MATLAB/VR toolbox simulates and visualizes the motion of objects in the virtual environments. The generated visual scenes are displayed at full screen mode on monitor for the operators. Figure 38 shows a visual scene, screen captured from the monitor. The virtual environment includes haptic platform (virtual end-effector and arm) shown by a ball connected to a thin grey cylinder, and authorized region, represented inside the virtual environments by intersecting solid

thick curves. The position of the ball inside the virtual environment is synchronized to the physical end-effector. As the participants move the physical end-effector, the ball also relocates inside the virtual reality.

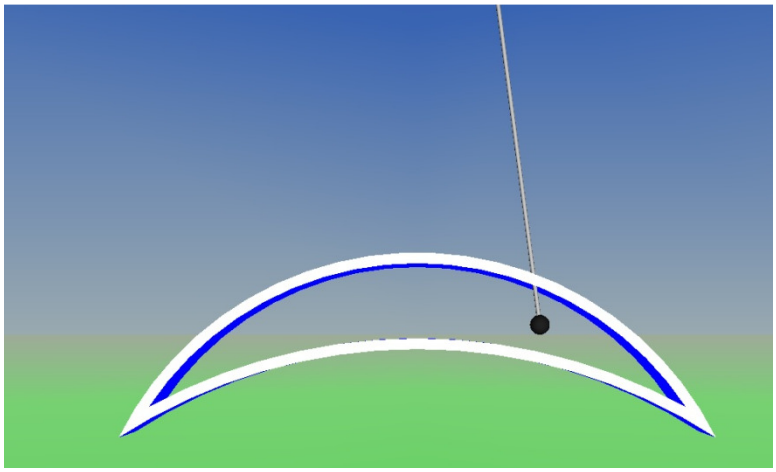

Figure 38: Virtual environment: blue color indicates that the end-effector is inside the authorized region

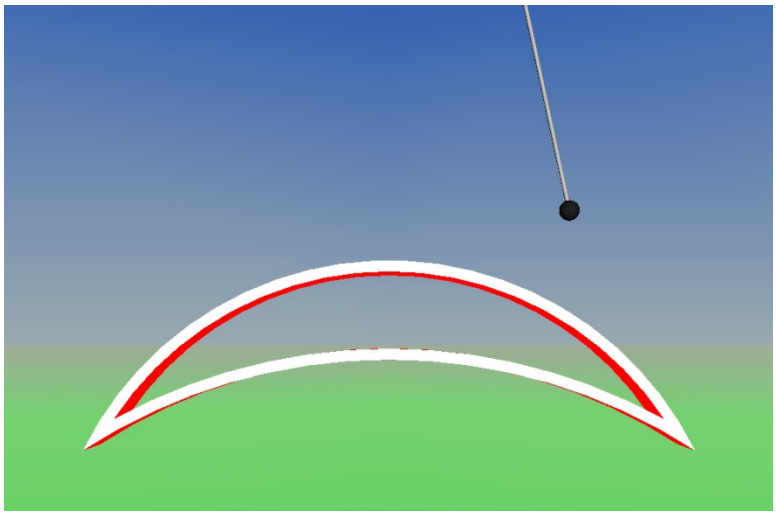

Figure 39: Virtual environment: red color indicates that the end-effector is outside the authorized region

To help operators to remain inside the authorized region, a visual warning feature is implement in the virtual environment by changing the color of the boundary from blue to red. Blue color (Figure 38) indicates that the operator is still inside the authorized region, however, the color of the walls turns into red (Figure 39) as soon as the end-

effector is pushed outside the region. In addition to this visual warning , the controller energizes the MR-Dampers to resist the motion in unwanted directions. Using the haptic and vision feedbacks, the operators can both feel and see the penetrations into prohibited regions and thus can change the direction and return the end-effector back to the authorized region.

4.2. Human Subject Tests

This human subject study is carried out to evaluate and compare the effects of different feedback conditions on operators' performances. This study has been categorized as 'Minimal Risk' and approved by the Director, Office of Research Ethics on behalf of the Research Ethics Board, in accordance with Simon Fraser University Policy (r20.01).

4.2.1. Participants/ Confidentiality

Experiments are conducted in the Advance Materials and Vibration Laboratory in the Mechatronic Systems Engineering (MSE) Department at Simon Fraser University (SFU). For each experiment, 10 Participants (nine male and one female) from SFU graduate students are recruited. Participants' ages ranged from 22 to 32 years old. Consent forms were collected from all participants in the experiments. To secure confidentiality, participants were anonymized by assigning a alphanumeric code to each one. Code numbers, participants' names and experimental data are securely stored in a password protected hard-disc. Digital data and paper files will be kept securely for a duration of 3 year, and then they will be destroyed.

4.2.2. Operation Risks to Human Subjects

Safety of the human subjects during the operations is indispensable criterion that needs to be proved to obtain approval from the research ethics board. Our haptic system has not the capability to apply force to the operator. The only force that participants feel is the resistance against motion. Any failure in the device terminates the operation. Also,

during the tests, participants can only touch the end-effector. Therefore, experiments are considered safe for the participants.

4.3. Experiments and Results

Participants are asked to explore the virtual environment by moving the interface end-effector inside the workspace. As it will be explained in sec 4.3.1 and 4.3.2, two series of tasks are designed to be performed by participants inside the virtual environment. All the participants are asked to complete the given tasks fast as accurate as possible. Position of the end-effector is recorded to study how accurately participants can perform the tasks. Box plots and method of within-subject analysis of variance (ANOVA) are used to study the results. ANOVA is a statistical technique that is used to investigate whether the different types of feedback conditions significantly affects the accuracy of the tasks [65].

During the experiments, participants can generally benefit from four different combinations of haptic and visual feedbacks:

*1) **HV**: With visual (Virtual reality) and haptic (resistance) feedbacks:*

In this condition, a participant can benefit from both visual and haptic feedback. Visual scenes of the virtual environment are displayed on a monitor. A ball inside the virtual environment represents the position of the end-effector in the interface workspace. If the end-effector is pushed outside of authorized region, the colors of walls turns into red. In this situation, the participant can see the position of ball relative to the authorized region, and change the direction to return the end-effector to the authorized regions. Also the participant can benefit from haptic feedback. Any deviation from the authorized region is associated with a resistance to the motion which helps the a participant to feel the deviation and correct the motion.

*2) **V**:With only visual feedback (Virtual reality):*

In this condition participants only benefit from the virtual reality. This means, by pushing the end-effector outside the authorized regions, MR-Dampers will not resist the

motion, but, the virtual reality walls on the screen will change into red, indicating the motion direction needs to be corrected. Therefore, the participant changes the directions to get the ball back inside the authorized region.

*3) **H**:With only haptic feedback (resistance):*

In this condition, participants can only benefit from haptic feedback. The screen is turned off in this case and participants have to correct the motion only based on the MR-Dampers resistance.

*4) **NO**: Without visual (Virtual reality) and haptic (resistance) feedbacks:*

In this condition the a participant should do the task without any help.

The aim of these conditions is to compare different feedback sources and investigate their effectiveness in guiding participants. In order to get the participants familiar with the different feedback sources, they were allowed to practice with the device in a training session prior to the actual test. After the training session, they were required to execute two series of tasks as follow:

4.3.1. Task 1: Circle Drawing Under Different Feedback Conditions

In the first task, the participants were asked to draw a circle with the help of different feedbacks. This task is designed to evaluate the effectiveness of the haptic feedback. This task is done in the four different conditions that was mentioned earlier.

First, participants drew a circle under *NO* feedback condition. They were allowed to draw any circle with any radius they like. The only restriction was the workspace limits of the interface. Then, a circle was fitted to the recorded points [66]. Based on the fitted circle (center (x_c, y_c) and radius (r)), a resistance map and a virtual environment were programmed. Figure 40 shows a virtual environment screen captured from monitor. In the figure, the fitted circle is shown by white color. As long as the end-effector is moving on the white circle, the inner and outer boundaries are displayed by blue color, however, blue color for each of the boundaries turns into red if the end-effector passes that boundary.

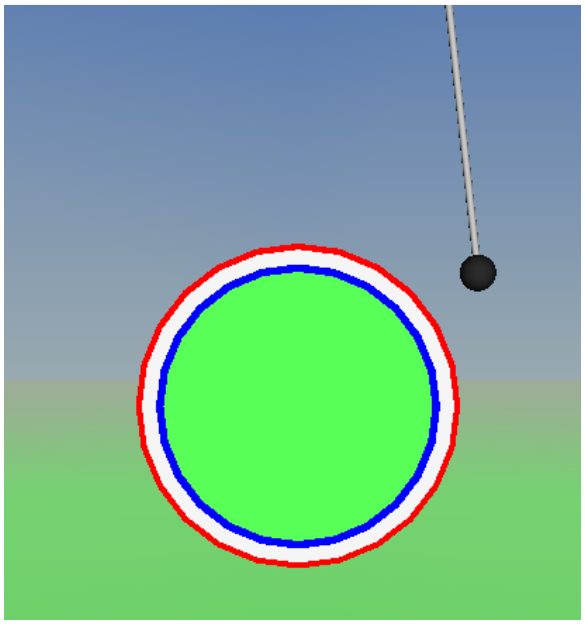

Figure 40: Virtual environment for Drawing Circle task, the end-effector is outside the outer boundary.

Circle drawing task was repeated under *V*, *H*, and *HV* conditions. To minimize the effect of order of the tests for the participants, the sequence of *V*, *H* and *HV* feedback conditions was randomized. Furthermore, a one minute rest was given to the participants between the task trials. A 75-second time threshold was considered as the maximum allowable time to finish the task trials and the ones that lasted longer than this threshold were repeated. Examples of experimental results for two participants (a and b) are shown in Figure 41 and 42.

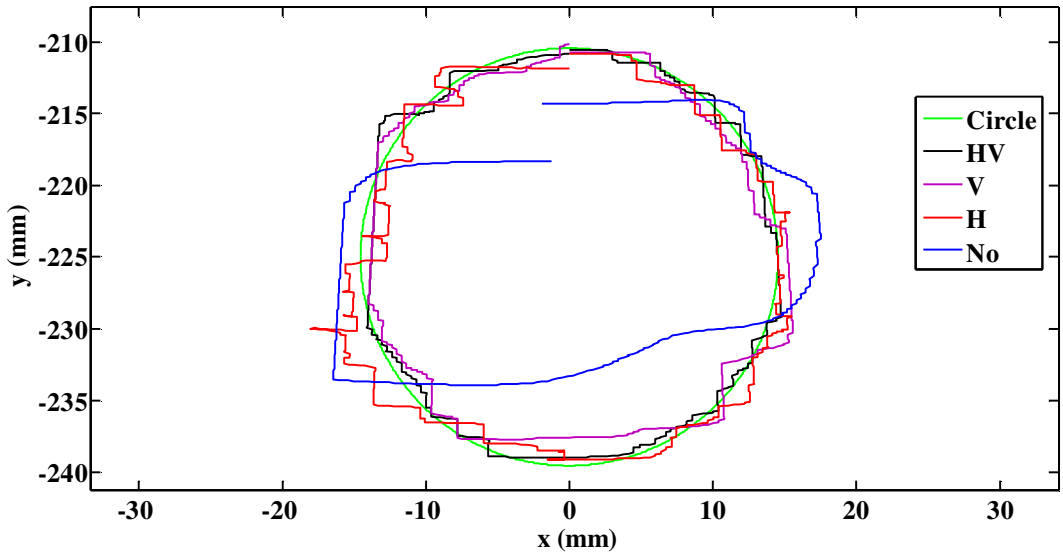

Figure 41: Experimental results for task 1 (participant a); HV :Haptic Visual feedback, V: Visual feedback, H: Haptic feedback, No: No feedback

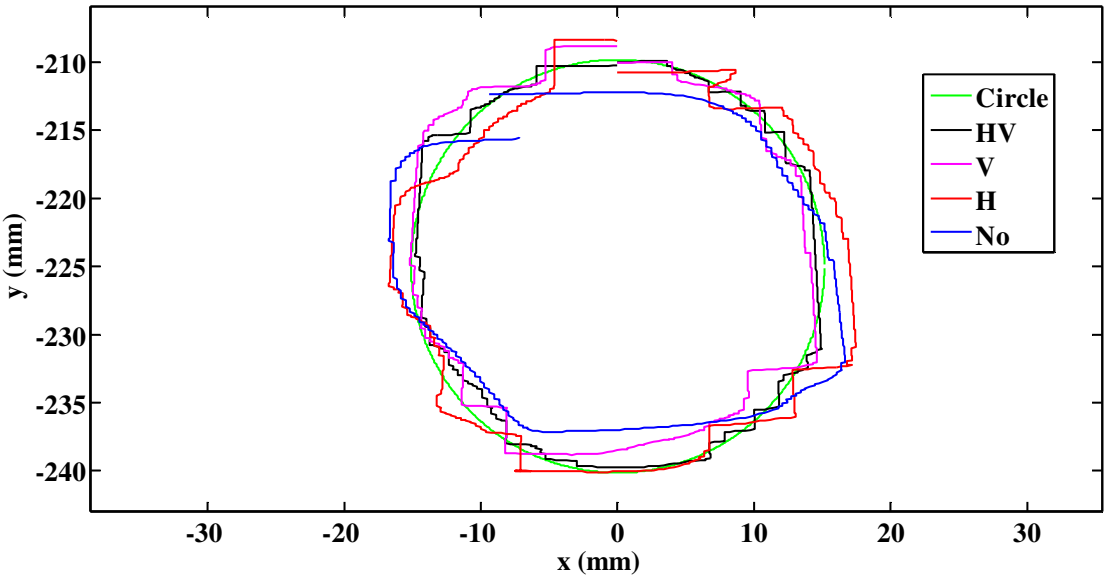

Figure 42: Experimental results for task 1 (participant b); HV :Haptic Visual feedback, V: Visual feedback, H: Haptic feedback, No: No feedback

To compare the effectiveness of the feedback conditions, the difference between fitted and drawn circle is chosen as the path error parameter. The sum of squared radial deviations are calculated to obtain the path error. The path errors are normalized with

the maximum recorded error. Normalized path errors for test trials shown in Figure 41 and 42 are listed in Table 3.

Table 3: Normalized errors of experiments shown in Figure 41 and Figure 42.

Feedback condition	Normalized error	
	Participant a (Figure 41)	Participant b (Figure 42)
NO	0.5139	0.2352
Haptic	0.1064	0.1492
Visual	0.1155	0.1333
Haptic Visual	0.0546	0.0625

Figure 43 shows a box plot of path errors across all participants for different feedback conditions. The mean normalized error across the participants are 0.698 for *NO*, 0.217 for *H*, 0.114 for *V* and 0.079 for *HV* feedback conditions. It can be observed from the results that error significantly decreases if the participant is guided by either visual or haptic feedbacks. Haptic feedback is not as effective as visual feedback, but it still can assist the participants to complete the task with an acceptable accuracy. Finally, the best results are obtained, when haptic and visual helps are combined.

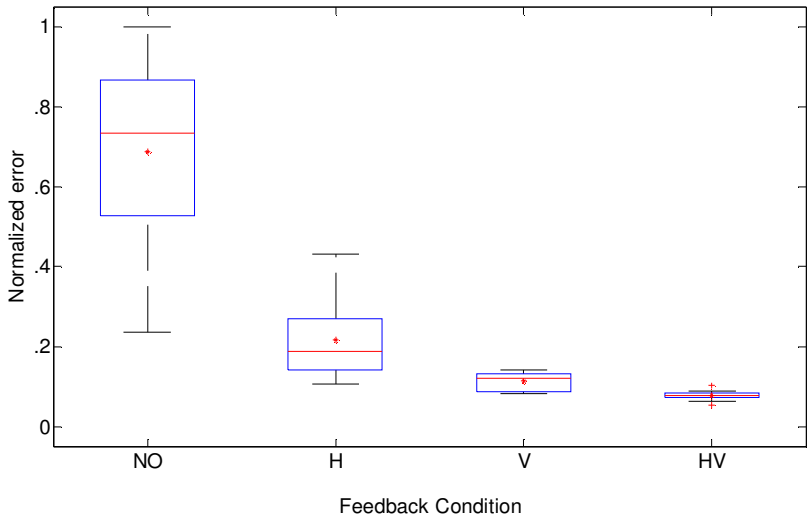

Figure 43: Box plot of participants normalized errors for task 1 under four feedback conditions. For each feedback condition, the central line marks the median, the asterisk shows the mean, the span of the box indicates the inter-quartile range, and the whiskers show the full range of the data.

In task 1, a two-way ANOVA is performed by using haptic feedback (present or absent) and visual feedback (present or absent) as the analysis factors. ANOVA results for task 1 is presented in table 4. In this table, *P* (significance level) is a probability value that determines how significantly ANOVA factors affect the results. Usually a factor is considered effective if its associated probability is less than an $\alpha = 0.05$ threshold. *P* value for haptic feedback is highly less than α which confirms that the provided haptic feedback positively and highly improves participants' performances.

Table 4: ANOVA results for task 1

ANOVA Factor	P (significance level)
Haptic	2.02 e-5
Visual	4.49 e-8

4.3.2. Task 2: Returning to Authorized Region from Prohibited Region

In the second task, end-effector was set initially out of authorized region. Participants were required to use the given feedback to find their way back to the region. To complete this task, participants needed to receive at least one of visual or haptic feedback, otherwise, the experiment was not doable. Thus, *NO* feedback condition was eliminated. Besides, *V* and *HV* feedbacks were modified and adopted as two new feedback conditions. In the *V* and *HV* conditions, the virtual environment is displayed on the monitor. The position of the ball and the color of the authorized region walls helps the operator to visually detect deviations from the authorized region. Participants can be further guider by displaying the shortest returning path and the closest point in the authorized region on the monitor. The new conditions are referred to as *V_gp* and *HV_gp* where gp stands for guiding path. As it can be seen in Figure 44, the green line shows the guiding path (gp) and the blue point indicates the closest point that would be reached if the guiding path is followed. The green line and the blue point appear only when the end-effector is outside of the authorized region. To ensure participants understands the meaning of the green line, at the same time, a descriptive sentence is also displayed on the monitor. It is excepted that *V_gp* and *HV_gp* conditions, enhances participants performance in returning to the authorized region.

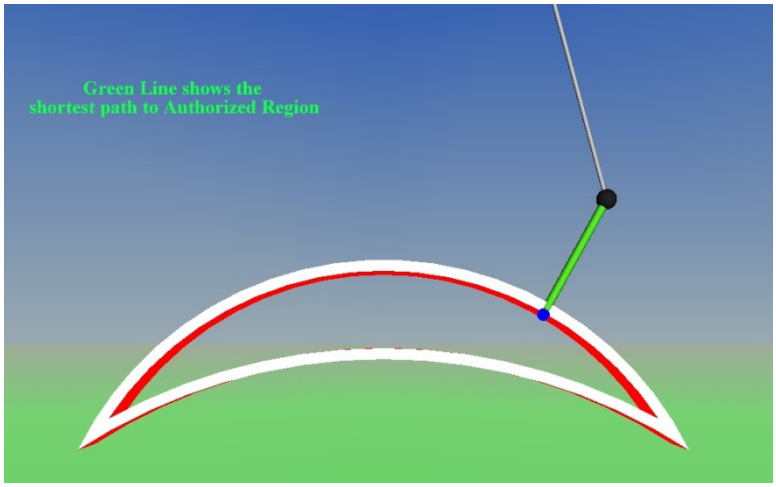

Figure 44: Virtual environment with guiding path (green line) and closest point indicator (blue point);end-effector is outside the authorized region.

The participants were asked to conduct the task under each of *V*, *H*, *HV*, *V_gp* and *HV_gp* feedback conditions in a random order. The time threshold to complete the task was set 20 seconds. The experiments that lasted longer than this threshold was repeated. Figure 45 shows an example of the experimental results for a participant. In this figure, the position history of the end-effector, from the starting point toward the authorized region is displayed for different feedback conditions.

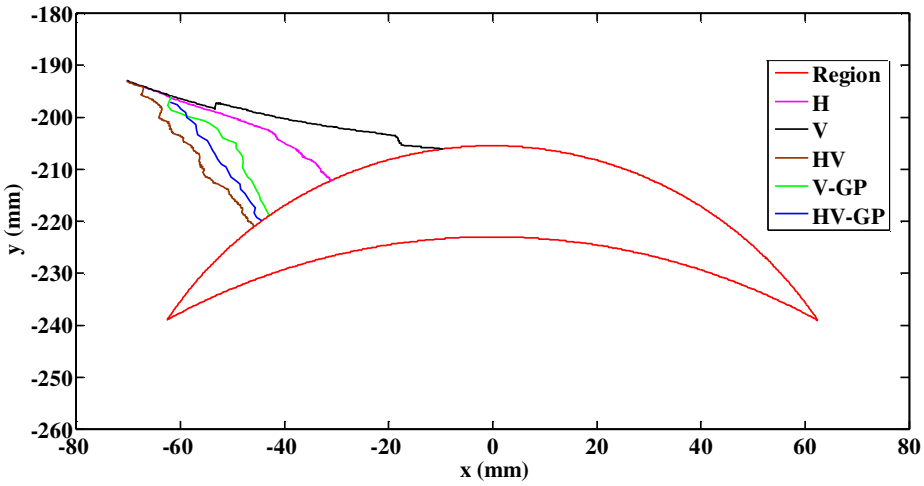

Figure 45: Experimental results for task 2; H: Haptic feedback, V: Visual feedback, HV: Haptic Visual feedback, V_GP: Visual feedback with guiding path, HV_GP: Haptic Visual feedback with guiding path,

To compare the effectiveness of feedback conditions, the path error (Equation 25) of participants performances under each condition is measured with respect to the ideal performance. The ideal performance in this task is to return to the authorized region exactly on the shortest path. Direction of shortest path at each location is the same as the maximum resistive force vector ($\boldsymbol{F}_{MRF}$). As explained in chapter 3, the direction of $\boldsymbol{F}_{MRF}$ vector at each location is (along the lines shown in Figure 24) toward the authorized region, and its magnitude is proportional to the position error from the resistance boundary. Equations 17 to 25 represent the derivation of the path error measurement used in our comparison.

The operator starts the task from starting point ($\boldsymbol{P_1} = \begin{bmatrix} x_1 \\ y_1 \end{bmatrix}$) and moves forward step by step until the authorized region is reached ($\boldsymbol{P_n} = \begin{bmatrix} x_n \\ y_n \end{bmatrix}$). The position history of the end-effector is given by a $2 \times n$ matrix ($\boldsymbol{P}$) as follow:

$$\boldsymbol{P} = [\boldsymbol{P_1} \quad \boldsymbol{P_2} \quad \cdots \quad \boldsymbol{P_{n-1}} \quad \boldsymbol{P_n}]_{2\times n} \qquad (17)$$

The displacement vectors ($\Delta\boldsymbol{P}$) between sequential points represent the $n-1$ motion steps from $\boldsymbol{P_1}$ to $\boldsymbol{P_n}$:

$$\Delta\boldsymbol{P} = [\Delta\boldsymbol{P_1} \quad \Delta\boldsymbol{P_2} \quad \cdots \quad \Delta\boldsymbol{P_{n-2}} \quad \Delta\boldsymbol{P_{n-1}}]_{2\times(n-1)} \qquad (18)$$

Where each column vector is obtained by:

$$\Delta\boldsymbol{P_i} = \boldsymbol{P_{i+1}} - \boldsymbol{P_i}\ , i = 1,2, \ldots, n-1 \qquad (19)$$

Also the absolute moved distances in the steps are

$$\boldsymbol{D} = [D_1 \quad D_2 \quad \cdots \quad D_{n-2} \quad D_{n-1}]_{1\times(n-1)} \qquad (20)$$

Where D_i is given by

$$D_i = |\Delta \boldsymbol{P_i}| \tag{21}$$

For each of points in position history matrix, the maximum resistive force vector ($\boldsymbol{F}_{MRF}$) is obtained.

$$\boldsymbol{F} = [\boldsymbol{F_{MRF_1}} \quad \boldsymbol{F_{MRF_3}} \quad \cdots \quad \boldsymbol{F_{MRF_{n-2}}} \quad \boldsymbol{F_{MRF_{n-1}}}]_{2\times(n-1)} \tag{22}$$

Where $\boldsymbol{F_{MRF_i}}$ is the maximum resistive force vector at point $\boldsymbol{P_i}$. The $\boldsymbol{F_{MRF_i}}$vector indicates the direction that if it was followed in the next step ($\boldsymbol{i}$ th step), zero error would have generated.

The deviation angles of displacement vectors ($\Delta\boldsymbol{P}$) with respect to maximum resistive force vectors ($\boldsymbol{F}$) are:

$$\boldsymbol{\varphi} = [\varphi_1 \quad \varphi_2 \quad \cdots \quad \varphi_{n-2} \quad \varphi_{n-1}]_{1\times(n-1)} \tag{23}$$

where

$$\varphi_i = \cos^{-1}\left(\frac{\Delta \boldsymbol{P}_i \cdot \boldsymbol{F}_{MRF_i}}{|\Delta \boldsymbol{P}_i| \cdot \left|\boldsymbol{F}_{MRF_i}\right|}\right), i = 1,2,\dots,n-1 \tag{24}$$

The inner product of $\boldsymbol{D}$ and $\boldsymbol{\varphi}$ matrices gives us the summation of path errors:

$$e = \boldsymbol{D} \cdot \boldsymbol{\varphi} \tag{25}$$

Once the path errors are calculated, they are normalized by the maximum recorded error in all the test trials. Table 5 includes the normalized errors for the experimental results shown in Figure 45.

Table 5: Normalized errors of experiments shown in Figure 45.

Feedback condition	Normalized error
H	0.4059
V	0.9264
HV	0.2498
H_gp	0.2506
HV_gp	0.1460

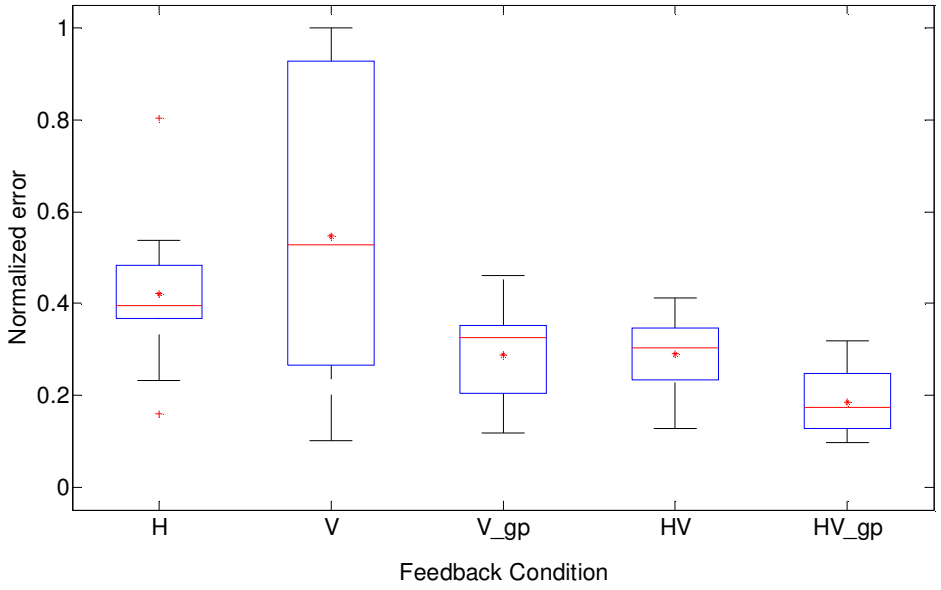

Figure 46: Box plot of participants normalized errors for task 2 under five feedback conditions. For each feedback condition, the central line marks the median, the asterisk shows the mean, the span of the box indicates the inter-quartile range, and the whiskers show the full range of the data.

The box plot of normalized errors for all the participants is also presented in Figure 46. The mean normalized error across the participants are 0.421 for Haptic (*H*), 0.547 for Visual (*V*), 0.288 for Visual with guiding path (*V_gp*), 0.291 for Haptic Visual (*HV*) and 0.185 for Haptic Visual with guiding path (*HV_gp*) feedback conditions. As it can be seen, the proposed haptic system is able to generate understandable haptic feedback. When haptic feedback is used as the only source of interacting information, the accuracy of the performances are comparable with visual feedback case which stands as successful proof for usefulness of haptic feedbacks in performing tasks.

Besides, the combination of visual and haptic feedback, increases the accuracy of the tasks. It is also found that displaying the return path on the monitor, enhances the accuracy in both of Visual and Haptic Visual feedbacks. *V_gp* and *HV_gp* conditions have produced 47.4 and 36.4 percent less errors comparing to *V* and *HV* conditions respectively.

For task 2, a three-way ANOVA analysis is performed. The selected factors for this analysis are haptic feedback (present or absent), visual feedback (present or absent) and guiding path (present or absent). The ANOVA results for task 2 are listed in table 6. The calculated significance levels for haptic feedback and guiding path reveal their effectiveness on participants performances again.

Table 6: ANOVA results for task 2

ANOVA Factor	P (significance level)
Haptic	2.38 e-3
Visual	2.16 e-1
Guiding Path	2.75 e-3

4.4. Conclusion

In this chapter, a human subject test is conducted to study the effectiveness of the proposed interface under different combination of haptic and visual feedback conditions. To provide visual feedback, A virtual reality environment is developed and loaded it into the controlling program. Two series of tasks are designed to be performed by the participants. In the first task, participants try to draw a circle as accurate and as fast as possible. In the second task, the end-effector is set initially outside of authorized region and the participants are asked to return back to it on the shortest path. Each of the tasks is conducted under different feedback conditions. It is observed that, haptic feedback provides enough sense of presence for the operators to finish the task and its performance is comparable with visual feedback condition. It is also found that the best results are obtained, if the operator can benefit from the haptic and visual feedbacks at the same time.

5. Conclusion

This Thesis is primarily motivated by a need to develop a simple, cost effective and more importantly safe haptic interface device. Haptic application is becoming more and more commonplace in various academic and industrial sectors such as medical robotics, CAD/CAM, video gaming and etc. The development of MR-Damper base haptic interface will extend the applications of Haptics by overcoming the safety concern of traditional active interfaces. Comparing to active actuators, MR-Dampers are only able to produce resistance and thus are totally safe. This Thesis focuses on developing an MR-Damper based haptic interfaces and a new haptic rendering algorithm called Digital Resistance Map (DRM) to control the interfaces. The general goal is to provide the operator with visual (Virtual reality) and haptic (resistance force) feedbacks to explore the virtual environment accurately.

In chapter 2, a preliminary study is conducted and the feasibility of replacing active actuators with MR-Dampers in haptic interfaces is verified. In this study, haptic based rehabilitation is selected as target application. The DRM is introduced as potential concept strategy for controlling MR-Dampers. Based on a given rehabilitation exercise, the DRM breaks down the haptic workspace into authorized and prohibited regions. In authorized region, the motion is set free while it will be resisted in the prohibited region.

In chapter 3, DRM concept is extended and introduced as a haptic rendering algorithm for semi-active interfaces. By generating understandable patterns of haptic scenes, the DRM guides operators to explore the programmed virtual environment. The DRM uses operator force and end-effector position as the input parameters to determine the magnitude and direction of resistance force needed to be generated by MR-Dampers. To implement the DRM, a polar planar haptic interface is fabricated and augmented with force and position sensors. It is experimentally proved that the proposed interface can effectively produce understandable haptic scenes.

Chapter 4 allocates to a human subject tests under different feedback conditions. Feedbacks are provided visually via monitors and/or haptically through haptic platform actuators (MR-Dampers). It is shown that presence of haptic feedback enhances participants accuracy in exploring the virtual environments and performing tasks.

As mentioned earlier, one of the most appealing application of our system is haptic based rehabilitation. For future work, it is possible to design a clinical trial to observe and study the effect of the proposed device on patients' healing process. To achieve this target, a virtual reality and resistance map will be generated based on a predefined rehabilitation exercise. During rehabilitation session, patients will be separated into two groups: group A and group B. First group (A) will do the exercises according to the traditional methods, while, the second group (B) will be allowed to use the device for doing their exercises. At the end of the session, functionality of patients from group (A) and group (B) will be compared and analysed. The results of such resourceful study can elucidate the benefits and drawbacks of the proposed approach.

References

[1] Witmer, Bob G., and Michael J. Singer. "Measuring presence in virtual environments: A presence questionnaire." *Presence* 7.3 (1998): 225-240.

[2] Srinivasan, Mandayam A., and Cagatay Basdogan. "Haptics in virtual environments: Taxonomy, research status, and challenges." *Computers & Graphics* 21.4 (1997): 393-404.

[3] Benali, Abderraouf, Paul Richard, and Philippe Bidaud. "A six dof haptic interface for medical virtual reality applications: design, control and human factors." *Virtual Reality, 2000.Proceedings.IEEE*.IEEE, 2000.

[4] Van der Linde, Richard Q., et al. "The Haptic Master, a new high-performance haptic interface." *Proc. Eurohaptics*. 2002.

[5] Kontarinis, Dimitrios A., and Robert D. Howe. "Tactile display of vibratory information in teleoperation and virtual environments." *Presence: Teleoperators and Virtual Environments* 4.4 (1995): 387-402.

[6] Hayward, Vincent, et al. "Haptic interfaces and devices." *Sensor Review* 24.1 (2004): 16-29.

[7] Wang, Qi, et al. "A haptic memory game using the STRESS 2 tactile display."*CHI'06 extended abstracts on Human factors in computing systems*. ACM, 2006.

[8] Wood, John, et al. "The design and evaluation of a computer game for the blind in the GRAB haptic audio virtual environment." *Proceedings of Eurohpatics* (2003).

[9] Wang, Qi, et al. "A haptic memory game using the STRESS 2 tactile display."*CHI'06 extended abstracts on Human factors in computing systems*. ACM, 2006.

[10] Zhu, Weihang, and Yuan-Shin Lee. "Five-axis pencil-cut planning and virtual prototyping with 5-DOF haptic interface." *Computer-Aided Design* 36.13 (2004): 1295-1307.

[11] Ha, S., et al. "Virtual prototyping enhanced by a haptic interface." *CIRP Annals-Manufacturing Technology* 58.1 (2009): 135-138.

[12] Mitsuishi, Mamoru, et al. "Master–slave robotic platform and its feasibility study for micro-neurosurgery." *The International Journal of Medical Robotics and Computer Assisted Surgery* (2012).

[13] Tholey, Gregory, and Jaydev P. Desai. "A general-purpose 7 DOF haptic device: applications toward robot-assisted surgery." *Mechatronics, IEEE/ASME Transactions on* 12.6 (2007): 662-669.

[14] Tse, Zion TszHo, et al. "Haptic needle unit for mr-guided biopsy and its control." *Mechatronics, IEEE/ASME Transactions on* 17.1 (2012): 183-187.

[15] Greer, Alexander D., Perry M. Newhook, and Garnette R. Sutherland. "Human–machine interface for robotic surgery and stereotaxy." *Mechatronics, IEEE/ASME Transactions on* 13.3 (2008): 355-361.

[16] Schirmbeck, E. U., et al. "Evaluation of haptic in robotic heart surgery."*International Congress Series*.Vol. 1281.Elsevier, 2005.

[17] McMahan, William, et al. "Tool contact acceleration feedback for telerobotic surgery." *Haptics, IEEE Transactions on* 4.3 (2011): 210-220.

[18] Asadi, E., Adam Hoyle, and Siamak Arzanpour. "Design of a Magnetorheological Damper-Based Haptic Interface for Rehabilitation Applications." *Journal of Intelligent Material Systems and Structures* 22.11 (2011): 1269-1277.

[19] Mali, Uros, NikaGoljar, and Marko Munih. "Application of haptic interface for finger exercise." *Neural Systems and Rehabilitation Engineering, IEEE Transactions on* 14.3 (2006): 352-360.

[20] Ferre, Manuel, et al. "Haptic device for capturing and simulating hand manipulation rehabilitation." *Mechatronics, IEEE/ASME Transactions on* 16.5 (2011): 808-815.[21] J. An and D. S. Kwon "Stability and performance of haptic interfaces with active/passive actuators theory and experiments", Int. J. Robot. Res., vol. 25, pp.1121, 2006

[22] Asadi, Ehsan, and Siamak Arzanpour. "Digital Resistance-Map Generation for a Magnetorheological Damper Based Platform for Rehabilitation Applications." ASME, 2011.

[23] Khademian, Behzad, and Keyvan Hashtrudi-Zaad. "Dual-user teleoperation systems: new multilateral shared control architecture and kinesthetic performance measures." *Mechatronics, IEEE/ASME Transactions on* 17.5 (2012): 895-906.

[24] Ahmadkhanlou, Farzad, Gregory N. Washington, and Stephen E. Bechtel. "The development of a five DOF magnetorheological fluid-based telerobotic haptic system." *The 15th International Symposium on: Smart Structures and Materials & Nondestructive Evaluation and Health Monitoring*. International Society for Optics and Photonics, 2008.

[25] Hayward, Vincent, and Karon E. MacLean. "Do it yourself haptics: part I."*Robotics& Automation Magazine, IEEE* 14.4 (2007): 88-104.

[26] Colgate, J. Edward, and J. Michael Brown. "Factors affecting the z-width of a haptic display." *Robotics and Automation, 1994.Proceedings., 1994 IEEE International Conference on*. IEEE, 1994.

[27] R. J. Adams and B. Hannaford, "Stable haptic interaction with virtual environments," IEEE Trans. Robot. Automat., vol. 15, pp.465-474, 1999.

[28] Kikuuwe, Ryo, et al. "Admittance and impedance representations of friction based on implicit Euler integration." *Robotics, IEEE Transactions on* 22.6 (2006): 1176-1188.

[29] Colombo, Roberto, et al. "Robotic techniques for upper limb evaluation and rehabilitation of stroke patients." *Neural Systems and Rehabilitation Engineering, IEEE Transactions on* 13.3 (2005): 311-324.

[30] Zhang, X., et al. "A novel passive path following controller for a rehabilitation robot." *Decision and Control, 2004.CDC. 43rd IEEE Conference on*.Vol. 5.IEEE, 2004.

[31] Prange, Gerdienke B., et al. "Systematic review of the effect of robot-aided therapy on recovery of the hemiparetic arm after stroke." *Journal of rehabilitation research and development* 43.2 (2006): 171.

[32] Stienen, Arno HA, et al. "Design of a rotational hydro-elastic actuator for an active upper-extremity rehabilitation exoskeleton." *Biomedical Robotics and Biomechatronics, 2008.BioRob 2008.2nd IEEE RAS & EMBS International Conference on*.IEEE, 2008.

[33] Munih, Marko, and TadejBajd. "'VI. 3.Rehabilitation Robotics." *Basic Engineering for Medics and Biologists: An ESEM Primer* 152 (2010): 353.

[34] Veras, Eduardo J., Kathryn J. De Laurentis, and Rajiv Dubey. "Design and implementation of visual-haptic assistive control system for virtual rehabilitation exercise and teleoperation manipulation." *Engineering in Medicine and Biology Society, 2008.EMBS 2008.30th Annual International Conference of the IEEE*.IEEE, 2008.

[35] Kikuchi, Takehito, et al. "Measurement of reaching movement with 6-DOF upper rehabilitation system "Robotherapist"." *Engineering in Medicine and Biology Society, 2008.EMBS 2008.30th Annual International Conference of the IEEE*.IEEE, 2008.

[36] Riener, R., T. Nef, and G. Colombo. "Robot-aided neurorehabilitation of the upper extremities." *Medical and Biological Engineering and Computing* 43.1 (2005): 2-10.

[37] Martin, Peter. *Real-time Neuro-fuzzy Trajectory Generation for Robotic Rehabilitation Therapy*. Diss. 2010.

[38] Shen, Y.,*Vehicle Suspension Vibration Control with Magnetorheological Dampers*, Diss, Waterloo University, 2005.

[39] Hoyle, A., S. Arzanpour, and Y. Shen. "A novel magnetorheological damper based parallel planar manipulator design." *Smart Materials and Structures* 19.5 (2010): 055028.

[40] Sapiński, Bogdan, and MaciejRosół. "MR damper performance for shock isolation." *Journal of Theoretical and Applied Mechanics* 45.1 (2007): 133-145.

[41] Reed, Matthew Robert. *Development of an improved dissipative passive haptic display*.Diss. Georgia Institute of Technology, 2003.

[42] Wereley, Norman M., Li Pang, and Gopalakrishna M. Kamath. "Idealized hysteresis modeling of electrorheological and magnetorheological dampers."*Journal of Intelligent Material Systems and Structures* 9.8 (1998): 642-649.

[43] Scilingo, Enzo Pasquale, et al. "A magnetorheological fluid as a haptic display to replicate perceived biological tissues compliance." *Micro technologies in Medicine and Biology, 1st Annual International, Conference On. 2000*. IEEE, 2000.

[44] Scilingo, Enzo Pasquale, et al. "Haptic displays based on magnetorheological fluids: design, realization and psychophysical validation." *Haptic Interfaces for Virtual Environment and Teleoperator Systems, 2003.HAPTICS 2003.Proceedings.11th Symposium on*.IEEE, 2003.

[45] Fisch, Avi, et al. "Development of an electro-rheological fluidic actuator and haptic systems for vehicular instrument control." *Proceedings of IMECE2003 ASME International Mechanical Engineering Congress and Exposition Washington, DC, USA*. 2003.

[46] Ahmadkhanlou, Farzad, et al. "The development of variably compliant haptic systems using magnetorheological fluids." *12th SPIE International Symposium, San Diego, CA*. 2005.

[47] Nikitczuk, Jason, Brian Weinberg, and Constantinos Mavroidis. "Control of electro-rheological fluid based torque generation components for use in active rehabilitation devices." *Society of Photo-Optical Instrumentation Engineers (SPIE) Conference Series*.Vol. 6174. 2006.

[48] Barreca, Susan, et al. "Treatment interventions for the paretic upper limb of stroke survivors: a critical review." *Neurorehabilitation and neural repair* 17.4 (2003): 220-226.

[49] Feys, Hilde, et al. "Early and repetitive stimulation of the arm can substantially improve the long-term outcome after stroke: a 5-year follow-up study of a randomized trial." *Stroke* 35.4 (2004): 924-929.

[50] Rahman, M. H., et al. "Development and control of a wearable robot for rehabilitation of elbow and shoulder joint movements." *IECON 2010-36th Annual Conference on IEEE Industrial Electronics Society*.IEEE, 2010.

[51] Zhang, Hong Hui, et al. "Dynamic response of magnetorheological fluid damper for automotive suspension and the influence by long-time standing-still." *Applied Mechanics and Materials* 105 (2012): 1689-1692.

[52] Milecki, Andrzej. "Investigation and control of magneto–rheological fluid dampers." *International journal of machine tools and manufacture* 41.3 (2001): 379-391.

[53] Choi, Kang-Min, et al. "Application of smart passive damping system using MR damper to highway bridge structure." *Journal of mechanical science and technology* 21.6 (2007): 870-874.

[54] Yang, G., et al. "Large-scale MR fluid dampers: modeling and dynamic performance considerations." *Engineering structures* 24.3 (2002): 309-323.

[55] Chang, Chih-Chen, and Paul Roschke. "Neural network modeling of a magnetorheological damper." *Journal of Intelligent Material Systems and Structures* 9.9 (1998): 755-764.

[56] An, Jinung, and Dong-Soo Kwon. "Modeling of a magnetorheological actuator including magnetic hysteresis." *Journal of Intelligent Material Systems and Structures* 14.9 (2003): 541-550.

[57] Çeşmeci, Şevki, and Tahsin Engin. "Modeling and testing of a field-controllable magnetorheological fluid damper." *International Journal of Mechanical Sciences*52.8 (2010): 1036-1046.

[58] Jung, Hyung-Jo, Billie F. Spencer Jr, and In-Won Lee. "Control of seismically excited cable-stayed bridge employing magnetorheological fluid dampers."*Journal of Structural Engineering* 129.7 (2003): 873-883..

[59] Franchi, Danilo, Alfredo Maurizi, and Giuseppe Placidi. "Characterization of a simmechanics model for a virtual glove rehabilitation system." *Computational Modeling of Objects Represented in Images* (2010): 141-150.

[60] Shaoqiang, Yuan, Liu Zhong, and Li Xingshan. "Modeling and simulation of robot based on Matlab/SimMechanics." *Control Conference, 2008. CCC 2008.27th Chinese*.IEEE, 2008.

[61] Kang, Hee-Jun, and Young-Shick Ro. "Robot manipulator modeling in Matlab-SimMechanics with PD control and online gravity compensation." *Strategic Technology (IFOST), 2010 International Forum on*.IEEE, 2010.

[62] Liu, Shao Gang, et al. "Path Planning and System Simulation for an Industrial Spot Welding Robot Based on SimMechanics." *Key Engineering Materials* 419 (2010): 665-668.

[63] Puccio, Francesca Di, Elena Franchi, and Federica Mattei. "SIMULATING HUMAN MOVEMENT IN SIMMECHANICS." *Journal of Biomechanics* (2008): S426-S426.

[64] Cho, Changhyun, Munsang Kim, and Jae-Bok Song. "Direct control of a passive haptic device based on passive force manipulability ellipsoid analysis."*International Journal of Control Automation and Systems* 2 (2004): 238-246.

[65] Hogg, Robert V., and Johannes Ledolter. Engineering statistics.Vol. 358. New York: MacMillan, 1987.

[66] Bucher, Izhak. Circle Fit: circfit.m. Computer Program. Mathworks, 2004.MATLAB m-file, 631 bytes.